

Examination of the performances of 22 CMIP6 ESMs on large scale changes in the atmosphere and oceans (North Atlantic, Arctic and North Pacific)

Zeliang Wang, Brendan DeTracey, Blair Greenan, David Brickman, Frederic Cyr, Peter S. Galbraith, Nadja Steiner and James Christian

Fisheries and Oceans Canada
Bedford Institute of Oceanography
1 Challenger Drive, Dartmouth, Nova Scotia, B2Y 4A2

2024

**Canadian Technical Report of
Hydrography and Ocean Sciences 376**



Canadian Technical Report of Hydrography and Ocean Sciences

Technical reports contain scientific and technical information of a type that represents a contribution to existing knowledge but which is not normally found in the primary literature. The subject matter is generally related to programs and interests of the Oceans and Science sectors of Fisheries and Oceans Canada.

Technical reports may be cited as full publications. The correct citation appears above the abstract of each report. Each report is abstracted in the data base *Aquatic Sciences and Fisheries Abstracts*.

Technical reports are produced regionally but are numbered nationally. Requests for individual reports will be filled by the issuing establishment listed on the front cover and title page.

Regional and headquarters establishments of Ocean Science and Surveys ceased publication of their various report series as of December 1981. A complete listing of these publications and the last number issued under each title are published in the *Canadian Journal of Fisheries and Aquatic Sciences*, Volume 38: Index to Publications 1981. The current series began with Report Number 1 in January 1982.

Rapport technique canadien sur l'hydrographie et les sciences océaniques

Les rapports techniques contiennent des renseignements scientifiques et techniques qui constituent une contribution aux connaissances actuelles mais que l'on ne trouve pas normalement dans les revues scientifiques. Le sujet est généralement rattaché aux programmes et intérêts des secteurs des Océans et des Sciences de Pêches et Océans Canada.

Les rapports techniques peuvent être cités comme des publications à part entière. Le titre exact figure au-dessus du résumé de chaque rapport. Les rapports techniques sont résumés dans la base de données *Résumés des sciences aquatiques et halieutiques*.

Les rapports techniques sont produits à l'échelon régional, mais numérotés à l'échelon national. Les demandes de rapports seront satisfaites par l'établissement auteur dont le nom figure sur la couverture et la page de titre.

Les établissements de l'ancien secteur des Sciences et Levés océaniques dans les régions et à l'administration centrale ont cessé de publier leurs diverses séries de rapports en décembre 1981. Vous trouverez dans l'index des publications du volume 38 du *Journal canadien des sciences halieutiques et aquatiques*, la liste de ces publications ainsi que le dernier numéro paru dans chaque catégorie. La nouvelle série a commencé avec la publication du rapport numéro 1 en janvier 1982.

Canadian Technical Report of
Hydrography and Ocean Sciences 376

2024

Examination of the performance of 22 CMIP6 ESMs on large scale changes
in the atmosphere and oceans (North Atlantic, Arctic and North Pacific)

by

Zeliang Wang¹, Brendan DeTracey¹, Blair Greenan¹, David Brickman¹, Frederic Cyr²,
Peter S. Galbraith³, Nadja Steiner⁴ and James Christian⁴

¹Fisheries and Oceans Canada

Bedford Institute of Oceanography

1 Challenger Drive, Dartmouth, Nova Scotia, B2Y 4A2

²Fisheries and Oceans Canada

Northwest Atlantic Fisheries Center

80 East White Hills Road

St. John's, Newfoundland and Labrador, A1C 5X1

³Fisheries and Oceans Canada

Maurice Lamontagne Institute,

Mont-Joli, Québec, G5H 3Z4

⁴Fisheries and Oceans Canada

Institute of Ocean Sciences

9860 West Saanich Road, Sidney, British Columbia, V8L 4B2

© His Majesty the King in Right of Canada, as represented by the Minister of the Department of Fisheries and Oceans, 2024

Cat. No.: Fs97-18/376E-PDF ISBN: 978-0-660-70195-0 ISSN: 1488-5417

Correct citation for this publication:

Wang, Z., DeTracey, B. Greenan, B., Brickman, D., Cyr, F., Galbraith, P., Steiner, N. and Christian, J. 2024. Examination of the performance of 22 CMIP6 ESMs on large scale changes in the atmosphere and oceans (North Atlantic, Arctic and North Pacific). Can. Tech. Rep. Hydrogr. Ocean. Sci. 376: v + 49 p.

TABLE OF CONTENTS

ABSTRACT	iv
RÉSUMÉ	v
1. Introduction	1
2. Validation of CMIP6 ESMs.....	2
2.1 Methodology and datasets	2
2.2 Atmospheric changes.....	3
2.2.1 Sea level pressure	3
2.2.2 Near surface air temperature	5
2.3 Ocean surface changes	6
2.3.1 SST of the North Atlantic Ocean	6
2.3.2 SST of the North Pacific Ocean	7
2.3.3 Sea ice of the Arctic Ocean	8
3. Model performance evaluation	10
4. Discussion.....	11
Acknowledgements:.....	13
References	13
Tables	16
Figures.....	21

ABSTRACT

Wang, Z., DeTracey, B. Greenan, B., Brickman, D., Cyr, F., Galbraith, P., Steiner, N. and Christian, J. 2024. Examination of the performance of 22 CMIP6 ESMs on large scale changes in the atmosphere and oceans (North Atlantic, Arctic and North Pacific). Can. Tech. Rep. Hydrogr. Ocean. Sci. 376: v + 49 p.

This study examines the performance of 22 CMIP6 models. Sea level pressure and 2m air temperature of the atmosphere component are compared with those from a reanalysis product. Sea surface temperature and sea ice from an observation-based ocean product are used to investigate the performance of the ocean component in these models. This study finds that the performance varies substantially between models and also between variables within one model. In general, these models do not represent sea level pressure well which is strongly related to the atmospheric circulation (winds), however, they well represent the 2m air temperature in terms of its long-term warming tendency over the historic time period. The multi-decadal variations of the sea surface temperature in the North Atlantic Ocean are captured by the majority of the models, however, they mostly fail to represent the dominant changes in the sea surface temperature in the North Pacific Ocean. This study suggests that the North Atlantic Ocean appears to be more predictable than the North Pacific Ocean. The declining trend in the summer Arctic ice area is reproduced, and some models have trends close to the observations. UKESM1-0-LL, CNRM-ESM2-1 and CESM2 are the three models with overall good performances for atmosphere, ocean and ice components.

RÉSUMÉ

Wang, Z., DeTracey, B. Greenan, B., Brickman, D., Cyr, F., Galbraith, P., Steiner, N. and Christian, J. 2024. Examination of the performance of 22 CMIP6 ESMs on large scale changes in the atmosphere and oceans (North Atlantic, Arctic and North Pacific). Can. Tech. Rep. Hydrogr. Ocean. Sci. 376: v + 49 p.

Cette étude analyse les performances de 22 modèles CMIP6. La pression au niveau de la mer et la température de l'air à 2 mètres de la composante atmosphérique sont comparées à celles d'un produit de réanalyse. La température de la surface de la mer et la glace de mer d'un produit océanique basé sur l'observation sont utilisées pour étudier la performance de la composante océanique dans ces modèles. Cette étude indique que les performances varient considérablement d'un modèle à l'autre et d'une variable à l'autre au sein d'un même modèle. En général, ces modèles ne représentent pas bien la pression au niveau de la mer, ce qui est fortement lié à la circulation atmosphérique (vents), mais ils représentent bien la température de l'air à 2 mètres en termes de sa tendance au réchauffement à long terme au cours de la période historique. Les variations pluridécennales de la température à la surface de la mer dans l'océan Atlantique Nord sont captées par la majorité des modèles, mais elles ne représentent généralement pas les changements dominants de la température à la surface de la mer dans l'océan Pacifique Nord. Cette étude suggère que l'océan Atlantique Nord semble plus prévisible que l'océan Pacifique Nord. La tendance à la baisse dans la zone de glace estivale de l'Arctique est reproduite, et certains modèles ont des tendances proches des observations. Les trois modèles UKESM1-0-LL, CNRM-ESM2-1 et CESM2 présentent de bonnes performances générales pour les composantes de l'atmosphère, de l'océan et de la glace.

1. Introduction

As a country surrounded by the three oceans, the North Atlantic, Arctic and North Pacific, Canada benefits from these oceans (e.g., subsistence harvesting, fisheries, recreational activities) and is impacted by changes in these oceans. What the future states of these oceans will be is of great interest not just to scientists but also to governmental bodies at various levels. Future changes in these oceans, e.g., currents, temperature, salinity, can significantly impact marine ecosystems including various endangered marine species, subsistence harvesting, economically important fisheries, and through those people's daily lives.

Climate models are essential tools to provide information on the evolution of climate quantities, their variability, and interactions with various components of the Earth System (Demory et al., 2020), and particularly on the future states of the climate of the ocean and atmosphere. The Coupled Model Intercomparison Project (CMIP) incorporates a wide range of climate models to provide enormous datasets for investigating climate change. The latest solutions from the sixth phase (CMIP6) are now available from the Earth System Grid Federation (ESGF; <https://esgf-node.llnl.gov/search/cmip6>), which provides projected changes in the ocean and atmosphere.

It is important to evaluate these climate models for Canada's three oceans over historical time periods before investigating the future states of these oceans. This evaluation will identify potential issues with the projected ocean states. Downscaling regional models has become an important tool to investigate detailed future conditions at regional scales. Because of the large computing resource requirements, downscaling regional ocean climate can only be performed for a very limited number of simulations with open boundary data and atmospheric forcing from CMIP results. This makes it difficult to assess the uncertainty associated with the regional projections. Hence, having a good understanding of the limitations imposed by the CMIP6 derived boundary conditions is very important.

Large-scale changes in the ocean and atmosphere are reflected in commonly-used indices, such as AMO (Atlantic Multi-decadal Oscillation; Loder and Wang, 2015) for the North Atlantic Ocean, sea-ice extent index for the Arctic Ocean (Wang et al., 2017), PDO (Pacific Decadal Oscillation; Wang et al., 2010) for the North Pacific Ocean, NAO (North Atlantic Oscillation; Wang et al., 2015, 2016, 2019) and AO (Arctic Oscillation; Wang et al., 2017) for the atmosphere over the North Atlantic and the Arctic, respectively. The continuing decrease of sea ice cover in the Arctic Ocean is seen as an important indicator of climate change. How well the CMIP6 models can represent these important indices is unknown. The sea ice in Arctic Ocean from the CMIP6 models have been reported in several studies, e.g., Shu et al. (2021), Notz and SIMIP (2020), Crawford et al. (2021), among others. Reader and Steiner (2022) provides links between trends in downscaling and CMIP models (CMIP5). In this study, the performance of the CMIP6 models on the Arctic sea ice will be investigated using multiple metrics.

In this study, we will evaluate the model performance on the large scale changes represented by climate indices in the three oceans, and also attempt to identify models which can better obtain the observed large scale variations in the ocean and atmosphere, which provides some guidance for climate downscaling models.

2. Validation of CMIP6 ESMs

This report focuses on investigating the performance of CMIP6 Earth System Models (ESMs) with respect to large scale features represented by climate indices in both atmosphere and ocean. The variables of sea level pressure, near surface air temperature and sea surface temperature are evaluated to help understand representation of large scale patterns in the CMIP6 models. Sea level pressure of the atmosphere not only reflects atmospheric circulation (wind) but is also used as a source to compute many important climate indices/teleconnections, such as the North Pacific Oscillation (NP or NPO), Arctic Oscillation (AO) and North Atlantic Oscillation (NAO). It is well known that wind plays an important role in driving ocean circulation and impacts upwelling/downwelling which could have significant biological consequences. Near surface air temperature (e.g. 2m above earth surface) is important to air-sea interaction, hence can impact ocean circulation and variations of ocean hydrographic conditions. Changes in sea surface temperature and sea ice are important quantities reflecting climate change. They are in direct contact with the atmosphere, are impacted by changes in the atmosphere, and impact the atmosphere as well.

2.1 Methodology and datasets

The Empirical Orthogonal Function (EOF) analysis is a common approach to investigate large scale changes and is, widely used in examining large scale phenomena in the atmosphere and ocean. Correlation and long-term trend, and bias analyses are used in examining model performance against reanalysis atmosphere/ocean products. Note that the historic simulations from CMIP6 ESMs are driven by historical GHG emissions, so these models develop their own interannual variability. This means that correlation with reanalysis data dominated by short term variability is not expected to be high. However, for data with significant inter-decadal variability, correlation analyses are useful because they can reveal the degree to which the CMIP6 simulations capture this long timescale variability.

Sea level pressure reanalysis (SLP) data and 2m air temperature (AirT) above the Earth surface are taken from NCEP/NCAR(<ftp.cdc.noaa.gov>: Projects/Datasets/ncep.reanalysis2.dailyavgs), with SLP and AirT spatial coverage for the northern hemisphere. SLP resolution is 2.5° in both longitude and latitude, and resolution of AirT is 1.875° in longitude and 1.889° in latitude.

Sea Surface Temperature (SST) and sea ice data are taken from HadISST (<https://www.metoffice.gov.uk/hadobs/hadisst/>). HadISST temperatures are reconstructed using a two stage reduced-space optimal interpolation procedure, followed by superposition of quality-improved gridded observations onto the reconstructions, to restore local detail. The sea ice fields are made more homogeneous by compensating satellite microwave-based sea ice concentrations for the impact of surface melt effects on retrievals in the Arctic. SSTs near sea ice are estimated using statistical relationships between SST and sea ice concentration (Rayner et al., 2003). The spatial coverage for the North Atlantic Ocean is 10.5°N to 65.5°N for latitude and 100.5°W to 29.5°E in longitude; resolution is 1° in both latitude and longitude. The spatial coverage for the North Pacific Ocean is 20.5°N to 64.5°N degrees in latitude and 105.5°E to 105.5°W in longitude with the same spatial resolution as for the North Atlantic Ocean. The spatial coverage for the Arctic Ocean is from 64.5°N to 90°N in latitude.

The northern hemisphere land-ocean temperature index (NH-ST) is taken from GISTEMP Team (2022) and Lenssen et al. (2019).

The following climate indices were downloaded from <https://psl.noaa.gov/data/climateindices/>:

- (1) The North Pacific Oscillation (NP/NPO) is a teleconnection pattern (Trenberth and Hurrell, 1994) and characterized by a north–south seesaw in sea-level pressure over the North Pacific Ocean.
- (2) The North Atlantic Oscillation (NAO; Hurrell, J.W., in the atmosphere over the North Atlantic. 1995; Jones, et al., 1997) describes changes in the strength of two recurring pressure patterns.
- (3) The Arctic Oscillation (AO; Zhou et al., 2001) is a climate index of the state of the atmospheric circulation over the Arctic.
- (4) The Atlantic Multi-decadal Oscillation (AMO; Enfield et al., 2001) is a coherent mode of natural variability occurring in the North Atlantic Ocean. It is based upon the average anomalies of sea surface temperatures (SST) in the North Atlantic basin, typically over 0°-80°N.
- (5) The Pacific Decadal Oscillation (PDO) is defined as the leading principal component of the North Pacific monthly sea surface temperature variability.

2.2 Atmospheric changes

2.2.1 Sea level pressure

Monthly SLP from NCEP and 22 CMIP6 models are examined using EOFs for the period of 1955-2014, which is the “historical” CMIP6 period. The 22 CMIP6 models have various model resolution, and before performing the EOF analysis, the SLP from each CMIP6 model was linearly interpolated onto NCEP grids.

Figure 2.2.1 shows the EOF1 patterns for SLP in NCEP and the CMIP6 models. The percentage of variance accounted for by this mode is indicated in each model panel. The EOF1 pattern of NCEP has three prominent centers, a generally negative one over the Asia-Europe continent, a positive one over the northern North Pacific Ocean, and another positive one over the northern North Atlantic Ocean but with smaller amplitude compared to the one over the North Pacific Ocean. The three-centered pattern in the NCEP EOF1 is mostly represented in the EOF1s of the 22 CMIP6 models, though their magnitudes, scales and relative differences among these centers differ from the NCEP EOF1. Both positive patterns are oval-shaped. We noticed that there is a small positive patch within the negative pattern in the NCEP EOF1, and this phenomenon is missing in all the CMIP6 EOF1s. The NCEP EOF1 accounts for 42% of the total variance, and percentages of variance represented by CMIP6 EOF1s range from 43% (GISS-E2-1G) to 66% (MIROC-ES2L).

The EOF2 patterns for NCEP and the 22 CMIP6 models are shown in Figure 2.2.2. The NCEP EOF2 has a three-centered pattern as well, but clearly different from the EOF1s, as expected. A negative patch is over the Arctic region, and two positive patches are over the northern North Pacific Ocean and mid-latitude North Atlantic Ocean. The shape of these two positive patches is east-west banded, which is different from the oval shaped one in EOF1, and the patch over the North Atlantic Ocean has a larger magnitude than the one over the North Pacific Ocean. The three-centered pattern in NCEP EOF2 is mostly captured by CMIP6 models, but differences between NCEP EOF2 and CMIP6 EOF2s are noticeable. The feature, that the magnitude of the positive patch over the North Atlantic Ocean is greater than that of the North Pacific Ocean in the NCEP EOF2, is mis-represented by several CMIP6 EOF2s, e.g., AWI-CM-1-1MR, CAMS-CM1-0, CanESM5, CESM2, CMCC-CM2-SRS, EC-Earth3, GISS-E2-1-G, IPSL-CM6A-LR,

MPI-ESM1-2-HR, MRI-ESM1-2-LR, NorESM2-LM, TaiESM1. More than half of the CMIP6 models fail to capture this feature. The NCEP EOF2 accounts for 12% of the total variance, and the variances accounted for by the CMIP6 EOF2s range from 5% (MIROC-ES2L) to 14% (GISS-E2-1-G), as indicated in Fig. 2.2.2.

The analysis of SLP was also intended to investigate possible connections between the principal components (PCs) and the climate teleconnection indices. The North Pacific Oscillation (NPO or NP), Arctic Oscillation (AO) and North Atlantic Oscillation (NAO) are three major climate indices in the northern hemisphere.

The top panel of Figure 2.2.3 shows the timeseries of the annual mean NCEP PC1 and NPO. A correlation coefficient of 0.70 between both suggests that the EOF1 reflects the NPO mode.

The winter (JFM) NAO has been found to significantly impact the circulation and hydrography of the North Atlantic Ocean (Wang et al., 2015, 2016, 2019). Timeseries of NCEP PC2 and winter NAO are shown in the middle panel of Figure 2.2.3, and clearly correlate with each other ($r=0.84$), suggesting that the EOF2 represents the NAO mode. It is clear that the prominent center with a negative patch over the Arctic Ocean is also a major feature of this mode and that the AO reflects SLP changes over the Arctic Ocean. The timeseries of the annual mean NCEP PC2 and AO are both shown in the bottom panel of Figure 2.2.3 with a correlation coefficient of 0.98. This means the EOF2 does represent both the NAO and the AO. Hamouda et al. (2021) reported these two are highly correlated, which is consistent with several other studies (references in Hamouda et al. 2021), though they found that this relationship changes with a warming climate. Our analysis for the 1955-2014 period further confirms the high correlation between AO and NAO, and indicate that both of them correspond to the NCEP EOF2.

One goal of this work is to identify which CMIP6 models may have better performance than others. As shown earlier, the EOF patterns from the CMIP6 models resemble those of NCEP. Since the NCEP PC1 and PC2 can represent those important climate indices, NP, NAO and AO, whether the PCs from the CMIP6 models can represent the NCEP PCs is of interest. Here, the correlation coefficients between NCEP PCs and PCs from the CMIP6 models are used as a measure of the model performance with respect to the reproducing the NCEP SLP. The correlation coefficients for SLP can be found in Table 2.2.1. Unlike the general similarity between NCEP EOFs and EOFs from CMIP6 models, the majority of the PCs from the CMIP6 models have no statistically significant correlation with NCEP PCs, which raises a concern for the CMIP6 models on representing the evolution of changes in the atmospheric circulation system associated with the SLP.

To further evaluate the model performance, these coefficients are normalized by the standard deviation of the 22 CMIP6 models' PC1/2, and the normalized coefficients are treated as model performance scores. These scores are ranked to represent model skills in presenting PCs of the NCEP SLP. This procedure is used in the evaluation of these models in this work. Figure 2.2.4 shows the 22 CMIP6 models' scores for PC1, PC2 representing the annual mean and for PC2 representing the winter mean (January, February, March - JFM). It is clear that the performance varies substantially among these models, also among the three coefficients in each model. For PC1, which represents the NPO, CNRM-CM6-1, CNRM-ESM2-1, UKESM1-0-LL, CAMS-CSM1-0, and MPI-ESM1-2-LR are the top 5 models. For PC2 (JFM), which corresponds to winter NAO, MPI-ESM1-2-HR, ACCESS-ESM1-5, UKESM1-0-LL, CNRM-ESM2-1, and EC-Earth3 are the top 5 models. MPI-ESM1-2-HR, UKESM1-0-LL, CAMS-CSM1-0, AWI-CM-1-

1-MR and ACCESS-ESM1-5 are the top 5 for PC2. It is noticed that the ranks for PC2 (JFM) and PC2 are similar in general, which is expected. Therefore, in the continued model evaluation, only the annual mean PC2 is evaluated.

2.2.2 Near surface air temperature

In this section, annual mean 2m air temperature (AirT) from NCEP and 22 CMIP6 models are examined. The EOF approach was applied to the NCEP AirT for the 1955-2014 period, and AirT data from the CMIP6 models was interpolated onto the NCEP AirT grid prior to applying the EOF.

Figure 2.2.5 shows the EOF1s for AirT for NCEP and the CMIP6 models. Unlike the patterns of the SLP EOFs which have prominent centers, the EOF1s for AirT do not have prominent centers in general, and the common feature of the EOF1s is that they mostly have positive patterns. Only a few models have clear negative patterns, e.g., CSMs-CSM1-0, GISS-E2-1-G, MIROC6, MIROC-ES2L. The NCEP EOF1 accounts for 29% of the total variance, and the variances accounted for by the CMIP6 models range from 15% (CAMS-CSM1-0) to 64% (EC-Earth3), where the majority of the models represents a larger variance than NCEP (Fig. 2.2.5).

The patterns of the AirT EOF2s from NCEP and CMIP6 models appear to be more complex than those of the respective EOF1s (Figure 2.2.6), though prominent centers show up in most of the CMIP6 models' EOF2s. The NCEP EOF2 shows four positive patches, mostly over continental land areas except for the one over the northwest of the North Atlantic Ocean; this feature is fully or partially captured by some models and missing in others. The NCEP EOF2 shows smaller changes over the North Pacific Ocean and North Atlantic Ocean compared with those over lands. In comparison, many of the CMIP6 models demonstrate strong variations over the oceans, mostly over the North Pacific Ocean. Only 11% of the total variance is accounted for by the NCEP EOF2, and 6% (ACCESS-ESM1-5 and EC-Earth3) to 18% (GISS-E2-1-G) of the total variances are accounted for by the CMIP6 models (indicated in Fig 2.2.6).

We found that the NCEP PC1 represents the northern hemisphere land-ocean temperature index (NH-ST; top panel of Figure 2.2.7) and has a correlation coefficient of 0.95. The NCEP PC2 correlates with the AO index ($r=-0.79$; bottom panel of Figure 2.2.7).

The correlation coefficients between NCEP PCs and PCs of the CMIP6 models are listed in Table 2.2.1, and it is clear that the NCEP PC1 is well represented by the majority of the CMIP6 models. Only one model (GISS-E2-1-G) has a correlation coefficient less than 0.5 ($r=0.29$), but the majority of the coefficients are larger than 0.8. In contrast, the correlation coefficients for PC2 are very small (Table 2.2.1), indicating this mode is poorly captured by these models.

Following the methodology described in 2.2.1 for model performance score, we calculated the model scores for PC1 and PC2 (Figure 2.2.8). The model scores for PC1 are mostly high except for GISS-E2-1-G. EC-Earth3, ACCESS-ESM1-5, AWI-CM-1-1MR, CanESM5, and ISPL-CM6A-LR are the top 5 models for PC1. As for PC2, the model scores are low and the top 5 models are UKESM1-0-LL, MPI-ESM1-2-HR, CNRM-ESM2-1, CESM2 and CNRM-CM6-1.

We also assessed the air temperature biases between the CMIP6 models and NCEP data over the 60-year period (1995 – 2014). The 60-year averaged bias was calculated for each model (listed in Table 2.2.1) and the bias patterns are shown in Figure 2.2.9. The majority of the CMIP6 models produce warm biases over the continental land areas, and cold biases over the North Pacific

Ocean and North Atlantic Ocean. The model biases for the northern hemisphere range from -1.3°C (UKESM1-0-LL) to 2.16°C (CMCC-CM2-SR5). A distinct feature of the bias patterns across the 22 models is an uneven distribution of the biases over land (warm) and ocean (cold).

2.3 Ocean surface changes

2.3.1 SST of the North Atlantic Ocean

Annual mean SST of the North Atlantic Ocean from HadISST and 22 CMIP6 models are investigated using EOFs for the historical period of 1955-2014. The SST from CMIP6 models were interpolated onto the HadISST grid prior to applying the EOF. Loder and Wang (2015) examined the SST EOF patterns for the North Atlantic Ocean and reported that both AMO and NAO signals can be represented by this EOF approach.

Figure 2.3.1 shows the EOF1 patterns from NCEP and the 22 CMIP6 models. The NCEP EOF1 pattern shows a prominent patch to the east of the Newfoundland, a slightly negative zone off the southern US coast and Gulf of Mexico, which is consistent with the EOF1 analysis in Loder and Wang (2015). This pattern was reported to be the AMO pattern in their study. The positive pattern in the subpolar region in the NCEP EOF1 is captured by the majority of the 22 CMIP6 models, and poorly or not represented by some, e.g., CAMS-CSM1-0, GISS-E2-1-G, MRI-ESM2-0, MPI-ESM1-2-HR.

The EOF2 patterns from NCEP and the CMIP6 models are shown in Figure 2.3.2. A tri-polar pattern is a key feature of the NCEP EOF2, with positive zones in the subpolar and tropical regions and a negative one in between them. This pattern was reported to be NAO related in Loder and Wang (2015). The tri-polar pattern is mostly reproduced in EOF2s of the CMIP6 models. Some are more apparent than others and the details in this tri-polar pattern vary among models. It appears that the tripolar pattern is mostly missing in the EOF2 pattern of CAMS-CSM1-0.

Loder and Wang (2015) investigated the relationship between the HadISST PCs with AMO and NAO. We followed their approach and investigated these relationships, shown in Figure 2.2.3. The AMO has a correlation coefficient of 0.91 with the HadISST PC1, and the HadISST PC2 correlates well with the AO ($r=-0.66$). We have discussed the close connection between the AO and NAO. Loder and Wang (2015) found the close relationship between HadISST PC2 and NAO. Here we show AO is also related to HadISST PC2, further confirming their interchangeability.

To examine the performance of each CMIP6 model, the correlation coefficients between CMIP6 models' PCs for SST and HadISST PCs are calculated and listed in Table 2.3.1. The CMIP6 models' PC1s are well correlated with the HadISST PC1 in general, indicating the AMO signal can be captured by these CMIP6 models. However, the PC2s of the CMIP6 models mostly fail in representing the HadISST PC2, which suggests the AO/NAO signals are not present in the CMIP6 models. This is consistent with the poor performance of CMIP6 models' SLP in representing the AO/NAO. The high performance of CMIP6 models on HadISST PC1/AMO is consistent with the CMIP6 models' good performance in representing the near surface air temperature (NCEP AirT PC1).

Following the methodology described in 2.2.1 for model performance scores, we calculated the model scores for the SST PC1 and PC2 (Figure 2.3.4). The model scores for PC1 are mostly high

except for IPSL-CM6A-LR and CAMS-CSM1-0. ACCESS-CM2, UKESM1-0-LL, MPI-ESM1-2-LR, EC-Earth3, ACCESS-ESM1-5, and AWI-CM-1-1-MR are the top 5 models for PC1 (SST). As for PC2, the model scores are low and the top 5 models are CNRM-ESM2-1, UKESM1-0-LL, AWI-CM-1-1-MR, CESM2, and MIROC6. Noticeably, UKESM1-0-LL and AWI-CM-1-1-MR are in the top 5 for both PC1 and PC2.

The models' SST biases relative to the HadISST data over the 60-year historical period are calculated and shown in Figure 2.3.5. The averaged biases over the whole North Atlantic Ocean are presented in each panel for the CMIP6 models, and listed in Table 2.3.1. The majority of the CMIP6 models produce a mean cold bias over the whole region, only ACCESS-ESM1-5, CESM2, CESM2-WACCM, NorESM2-LM and TaiESM1 have mean warm biases. The largest cold bias is from CAMS-CSM1-0 (-1.71°C). Figure 2.3.5 shows that the distribution of the biases over the whole North Atlantic Ocean can vary significantly from cold to warm, which means warm biases can be dominating at local scales, despite a mean cold biases for the whole of the North Atlantic Ocean, and vice versa.

2.3.2 SST of the North Pacific Ocean

Following the same procedure for the North Atlantic Ocean, annual mean SST for the North Pacific Ocean from HadISST and the 22 CMIP6 models are investigated. The SST from the CMIP6 models were interpolated onto HadISST grids.

The SST EOF1 and EOF2 patterns and their PCs were obtained using the EOF analysis approach. It was found that the NCEP EOF1 pattern is mostly present in the EOF2 patterns of the CMIP6 models, while the NCEP EOF2 corresponds to the EOF1 of the CMIP6 models. Exceptions are ACCESS-CM2, MIROC6 and MIROC-ES2L, whose patterns are not switched. Hence in this analysis, we switched those CMIP6 models' modes to be consistent with the corresponding HadISST mode, and those PCs are switched as well. Hereafter, EOFs and PCs are the switched EOFs and PCs, if not specified.

Figure 2.3.6 shows the SST EOF1s from HadISST and the CMIP6 models. The HadISST EOF1 shows a negative pattern in the west and a positive pattern in the east, as is the typical PDO pattern. This pattern is shown in the EOF2s of the CMIP6 models in general, though differences are noticeable, e.g., the size/shape of the negative/positive patches. The HadISST EOF1 accounts for 31% of the total variance, and the variances accounted for by EOF1s from the CMIP6 models range from 14% (AWI-CM-1-MR) to 42% (MIROC-ES2L) (indicated in Fig. 2.3.6).

A general positive pattern is a key feature of the HadISST EOF2 (Figure 2.3.7), and this general positive pattern is mostly captured by the CMIP6 models, with some showing stronger positive regions than the HadISST EOF2. Some also show negative zones in this mode. The HadISST EOF2 accounts for 18% of the variance, the CMIP6 models' SST EOF2s variances account for 14% (ACCESS-CM2 and MIROC6) to 49% (CESM2-ESM2-1). The high percentage of the represented variance in many CMIP6 models is due to fact that these EOF2s are from their original EOF1s.

Unsurprisingly, the HadISST PC1 is strongly correlated with the PDO index ($r=0.92$; top panel of Figure 2.3.8), and consistent with the PDO pattern shown in EOF1. The HadISST PC2 is found to correlate with NH-ST ($r=0.74$; bottom panel of Figure 2.3.8), suggesting the pattern reflects the general surface temperature variations of the northern hemisphere.

Correlation coefficients between CMIP6 model's PCs for SST and HadISST PCs are calculated and listed in Table 2.3.1. The CMIP6 models' PC1s are poorly correlated with the HadISST PC1, suggesting the PDO signal is not reasonably captured by the CMIP6 models. However, the majority of the PC2s of the CMIP6 models have moderate to high correlation with the HadISST PC2, demonstrating that these models can represent the general warming trend seen in the NH-ST for the northern hemisphere, and this is consistent with the models' good performance for the near surface air temperature (EOF1/PC1 of the AirT).

For the model performance score, we calculated the model scores for the North Pacific SST PC1 and PC2s (Figure 2.3.9). The model scores for PC1 are mostly very low. EC-Earth3, AWI-CM-1-1MR, ACCESS-CM2, CESM2 and MPI-ESM1-2-HR are the top 5 models for PC1. As for PC2, the model scores are generally high, and the top 5 models are UKESM1-0-LL, EC-Earth3, AWI-CM-1-1-MR, TaiESM1 and CNRM-ESM2-1. Noticeably, EC-Earth3 and AWI-CM-1-1-MR are in the top 5 for both PC1 and PC2.

Figure 2.3.10 shows models' biases relative to the HadISST data over the 60-year historical period. The averaged biases over the whole North Pacific Ocean are presented in each panel for the CMIP6 models, and listed in Table 2.3.1. Consistent with the North Atlantic Ocean, the majority of the CMIP6 models reproduce the mean cold bias over the whole region. Only ACCESS-ESM1-5, CESM2, CESM2-WACCM, CMCC-CM2-SR5 and CNRM-ESM2-1 have mean warm biases. The largest cold bias is from GISS-E2-1-G (-1.78°C). Similarly to the North Atlantic Ocean, the distribution of the biases over the whole North Pacific Ocean can vary greatly from cold to warm, and warm bias can be clearly seen at local scales.

To investigate the models' SST bias evolution over the 1955-2014 period, we divided this 60-year period into six decades, and the mean model bias in each decade was calculated for each CMIP6 model for the North Atlantic Ocean and the North Pacific Ocean, separately. We resorted to violin plots to present the time-varying model biases and to show the mean bias distribution across the 22 CMIP6 models (Figure 2.3.11).

The mean model bias from the 22 CMIP6 ESMs (indicated by horizontal bars in Figure 2.3.11) from the 1st decade (1st Dec) to the 6th decade (6th Dec) is a cold bias for both the North Atlantic Ocean and North Pacific Ocean. The mean model bias for the North Atlantic Ocean increases from the 1st decade to the 4th decade, then decreases. In contrast, the mean model bias shows a gradual increase in trend for the North Pacific Ocean.

2.3.3 Sea ice of the Arctic Ocean

In this section, we evaluate the model performance for Arctic sea ice. The sea ice concentration from HadISST was compared with those from the CMIP6 models. Note that sea ice data from CNRM-CM6-1-HR had quality issues at the time of preparation for this report and is excluded. We selected March and September, to represent the highest winter and lowest summer ice cover in the Arctic Ocean. Hereafter winter means March and summer means September.

Figure 2.3.12 shows the sea ice concentration in March of 2014 from HadISST and the CMIP6 models. The feature of high ice concentrations in the Arctic Mediterranean water in HadISST can be captured by all the CMIP6 models, and the differences between the ice from HadISST and CMIP6 models are dominantly in the marginal ice zones, such as Baffin Bay and the Nordic Sea.

The September 2014 summer ice concentrations from HadISST and CMIP6 models are shown in Figure 2.3.13. Unlike the general similarity between the HadISST ice cover and those of CMIP6 models, there are significant differences between the HadISST ice concentration and the ice concentrations of the CMIP6 models, not just in the ice edges, but also in the central Arctic region where the HadISST ice has high ice concentration and a narrow rim of low ice concentration around it. The shape of the high ice concentration area is mostly mis-represented by the CMIP6 models. The CMCC-CM2-SR5 does not have any high ice concentration area in the central Arctic Ocean. The ice extents from HadISST and CMIP6 models also appear to be significantly different.

To present quantitative assessment of the model performance on sea ice, ice areas are calculated for the HadISST and CMIP6 models for the two representative seasons, winter and summer. To investigate the evolution of ice area in winter and summer over the 60-year period, correlation coefficients between the HadISST ice area and ice areas of the CMIP6 models were calculated, and listed in Table 2.3.2. The correlation coefficients for winter vary significantly from model to model. However those for the summer are moderate to high, suggesting these models can better represent ice changes over time in summer than those in winter.

Model scores representing ice area in winter and summer in terms of ice area evolution from 1955 to 2014 are presented in the top panel of Figure 2.3.14. The top 5 models for winter ice area are CNRM-ESM2-1, EC-Earth3, UKESM1-0-LL, NorESM2-LM, and CNRM-CM6-1. The top 5 ones for summer are EC-Earth3, CESM2, IPSL-CM6A-LR, MPI-ESM1-2-HR and MPI-ESM1-2-LR. Since these two metrics are independent for either season, it is necessary to evaluate the model performance for the two seasons together. In the bottom panel of Figure 2.3.14, the summation of the two metrics is used to represent model's performance on the two seasons together, and the top 5 models in this measure are EC-Earth3, CESM2, MPI-ESM1-2-LR, CNRM-CM6-1 and AWI-CM-1-MR.

Ice area bias and trends are of great interest in terms of evaluating these models' performance. The ice area biases between HadISST and CMIP6 models for the two seasons and their trends are shown in Table 2.3.2.

Consistent with the previous approach in the calculation of model score, the model error scores are calculated (top panel of Figure 2.3.15), and their rankings are shown as well. Note: the rankings are for model performance: smaller error score means better model performance. The combined error scores were also calculated and shown in the bottom panel of Figure 2.3.15. In terms of combined model bias on ice area of the two seasons, the top 5 best CMIP6 models are MIROC6, ACCESS-ESM1-5, MIROC-ES2L, MPI-ESM1-2-LR and CESM2-WACCM.

Following the same approach for ice area bias, the biases for ice area trends of winter and summer were calculated, and then the error scores were calculated and shown in the top panel of Figure 2.3.16. The combined trend error scores are shown in the bottom panel in the same figure. The top 5 best CMIP6 models for representing trends for the two season are CanESM5, TaiESM1, MRI-ESM2-0, CESM2-WACCM, and CNRM-CM6-1.

We noticed that the sea-ice trends for winter and summer are significantly different in HadISST, and the ratio between the summer trend and winter trend is another quantity of interest (Table 2.3.2). The HadISST trend ratio (summer/winter) is 3.8. The errors on the trend ratio and the

error scores are shown in Figure 2.3.17. In this measure, the top 5 CMIP6 models are GISS-E2-1-G, CanESM5, MRI-ESM1-2-LR, CESM2, and CNRM-CM6-1.

3. Model performance evaluation

In this section, we attempt to evaluate the performance of the CMIP6 models based on results from Section 2. The strategy to evaluate these models is: (1) for the atmosphere, calculate the total scores for SLP and AirT respectively (combined scores of PC1 and PC2), and then calculate the combined score of SLP and AirT to represent the total score of the atmospheric component of the CMIP6 models; (2) for ocean SST, calculate total scores for the North Atlantic Ocean and North Pacific Ocean, respectively, then calculate the combined score for the two oceans. The model performance on sea ice was already presented in section 2.3.3. Based on several measures assessing the model performance on sea ice, we found that there is a general lack of consistency among these measures. Since the decreasing sea ice cover in the summer time is a significant indicator for climate change we used the trend of summer ice area as the measure for model performance for the Arctic Ocean (Figure 2.3.16).

Figure 3.1 shows the model scores for SLP and AirT (top panel) and the combined scores (bottom panel). The score for SLP of each model is lower than that of AirT, which suggests that near surface air temperature is better represented by the CMIP6 models than the sea level pressure which is related to the atmospheric circulation. The top 5 models for SLP are UKESM1-0-LL, CNRM-ESM2-1, CNRM-CM6-1, CAMS-CSM1-0 and MPI-ESM1-2-HR. The top 5 models for AirT are UKESM1-0-LL, CMCC-CM2-SR5, CNRM-CM6-1-HR, and CESM2-WACCM. The top 5 models for the atmospheric component of the CMIP6 models are UKESM1-0-LL, CNRM-ESM2-1, MPI-ESM1-2-HR, CEMS2, and CNRM-ESM2-1.

For the performance on SST (Figure 3.2), there is a general tendency that the model performance for the North Pacific Ocean is better than that for the North Atlantic Ocean. We need to point out that the calculation of scores for the North Pacific Ocean was based on switched EOF modes, and the observed dominant PDO mode is presented in the second mode of the majority of the CMIP6 models, and the warming signal in the HadISST second mode is in the first mode of many CMIP6 models. Hence the relative model performance for these two oceans represented in Figure 3.2 is unrealistic. The top 5 models for the North Atlantic Ocean are UKESM1-0-LL, AWI-CM-1-1-MR, CNRM-ESM2-1, CESM2-WACCM, and CESM2. The top 5 models for the North Pacific Ocean are EC-Earth3, AWI-CM-1-1MR, CESM2, CNRM-ESM2-1, and CNRM-CM6-1. The top 5 models for the presentation of SST of the two oceans are AWI-CM-1-1-MR, EC-Earth3, UKESM1-0-LL, CNRM-ESM2-1, and CESM2.

Table 3.1 lists the rankings of model performance for the three oceans. We calculated the averaged ranking scores (the mean of the ranking numbers for the three oceans) for the CMIP6 models to represent the overall performance of the CMIP6 models for the three oceans. We found that the top 5 models on representing all three oceans are UKESM1-0-LL, CNRM-ESM2-1, AWI-CM-1-1-MR, CESM2, and EC-Earth3. The top 5 models for the atmospheric component are UKESM1-0-LL, CNRM-ESM2-1, MPI-ESM1-2-HR, CEMS2, and CNRM-ESM2-1. It is clear that UKESM1-0-LL, CNRM-ESM2-1 and CESM2 are in the top 5 models of ocean and atmosphere components.

4. Discussion

This study evaluates 22 CMIP6 models with respect to their representation of observed SLP, AirT from NCEP/NCAR for the northern hemisphere, SST from HadISST for the North Atlantic Ocean and North Pacific Ocean, and sea ice from HadISST for the Arctic Ocean.

Our analyses of the NCEP/NCAR sea level pressure and 2m air temperature data show that the NPO and AO/NAO can be represented by PC1 and PC2 of the SLP, respectively, and AirT PC1 is closely linked with the northern hemisphere land-ocean surface temperature index (NH-ST), while its PC2 is related to the AO/NAO events. We noticed both the low pressure system (negative pattern) in the SLP EOF2 (Figure 2.2.2) and the cold pattern in the AirT EOF2 (Figure 2.2.6) cover the entire Arctic, and this could be the reason why the AirT PC2 is related to the AO/NAO.

The analysis of SLP from the CMIP6 models clearly shows that these models cannot capture the temporal variations of the sea level pressure indicated by the NPO or AO/NAO which are the dominant atmospheric events over the North Pacific, Arctic and North Atlantic, respectively, though the EOF1 and EOF2 patterns from these models are consistent with those from NCEP/NCAR in general (Table 4.1).

Unlike for SLP PCs, the majority of the AirT PC1s of the CMIP6 models well represent PC1 of the NCEP/NCAR AirT, though their PC2s fail in representing the NCEP/NCAR AirT PC2. This is expected since the AirT PC2 is related to SLP PC2 (AO/NAO). However, though the general warm patterns can be seen in the NCEP/NCAR AirT EOF1 and the majority of CMIP6 models, differences in the details of this mode between the NCEP/NCAR EOF1 and modeled EOF1s are obvious. The correlation coefficients between the NCEP/NCAR AirT EOF1 and EOF1s of these models are generally much lower than those for the SLP EOF1 (Table 4.1). Differences in the AirT EOF2 patterns are even larger in most of the CMIP6 models, and show mostly low (or negative) correlations (Table 4.1). Exceptions are CNRM-CM6-1 ($r=0.74$), CNRM-ESM2-1 ($r=0.76$), MPI-ESM1-2-HR ($r=0.66$), CNRM-CM6-1-HR ($r=0.68$), IPSL-CM6A-LR ($r=0.69$) and UKESM1-0-LL (0.68).

Thermodynamics and dynamics are the two fundamental principles of physics governing climate models (Shepherd, 2014). Our analyses of the SLP and AirT suggest that the temporal evolution of the near surface air temperature (AirT PC1), presumably resulting from the thermodynamics, is well represented by climate models, but the evolution related to the dynamics (atmospheric circulation) is not reasonably represented (AirT PC2). This is in line with the general understanding of the thermodynamics and dynamics in climate models. The good performance of AirT PC1s of the CMIP6 models and the not-so-good performance of their EOF1s are of a big contrast. And there is also a big contrast in the SLP, which shows good performance on EOF patterns, but bad on PC performance.

The AMO which is represented by the PC1 of the HadISST data for the North Atlantic Ocean, and the SST variations represented in HadISST PC1 are well captured by the PC1s of the CMIP6 models. This suggests that the long-term variability of the SST in the North Atlantic Ocean can be reproduced by these models in general. However, the HadISST PC2, which is related to AO/NAO events, cannot be well captured by the models. Notably, both the HadISST EOF1 and EOF2 patterns can be roughly seen in the EOFs of these models in general (Table 4.1), though differences in details are noticeable. Figure 4.1 shows the relation between the AMO and NH-

ST. They have a correlation coefficient of 0.69, and the detrended AMO and NH-ST have a correlation of 0.85. We suggest that the AMO is part of surface land-ocean temperature changes represented by NH-ST, and as mentioned earlier, the PC1 or the AirT is consistent with NH-ST. Hence we suggest the long-term variations of SST in the North Atlantic Ocean are related to the long-term air temperature changes which are impacted by green-house-gas emission. To this extent, the SST of the North Atlantic Ocean is kind of predictable, which is consistent with what was suggested by Smith et al. (2020) who reported that the North Atlantic climate is far more predictable than models imply.

The PDO is the dominant SST event in the North Pacific Ocean, which is seen in the PC1 of the HadISST dataset. The general warming trend in SST is shown in the HadISST PC2, and this is part of the land-ocean surface temperature of the northern hemisphere (NH-ST). This is in contrast with the North Atlantic Ocean in which the long-term warming trend is captured by its PC1. In the majority of the CMIP6 models' solutions, the PDO pattern is in the SST second EOF2 mode (the un-switched one), and the general warming pattern seen is EOF1. This suggests the warming SST events are generally overestimated by these models, overtaking the actual more important PDO events. Hence we suggest that the North Pacific Ocean is less predictable than the North Atlantic Ocean.

Assessing the ice cover in the Arctic Ocean is complicated and the measures applied in this study (Table 2.3.2) do not provide consistent results. Since summer ice cover is a commonly adopted indicator to demonstrate the impact of climate changes – the warming impacts, we use this measure as the lead quantity to assess these models. The summer ice areas from these models have generally moderate to high correlations with the ice area from HadISST. The declining trend in ice area is seen in all models, and many models produce the trends close to the HadISST summer ice trend (Table 2.3.2). Surface heating is the main cause for the ice melting, and the CMIP6 models can well represent the evolving warming with time shown in AirT PC1, hence the sea ice cover in the Arctic Ocean is predicable in general by these models, though performance of these model vary (Figures 2.3.14 - 2.3.17).

The steady increasing GHG emissions since early 20th century were observed and reported (Boden et al., 2017). This increasing trend is expected to reflect on the changes in the air and oceans. When there is a trend in the investigated variable related to the increasing trend in the GHG emissions, it can be captured by the correlation approach used in this study. This could be another reason why the PCs in the air temperature and SST with obvious trends, together with the winter and summer ice areas which have clear trends, all have good correlations with observations besides the thermodynamics mentioned above. The low correlations in PCs without clear trends between the CMIP6 models and observations could be in part from the different (unrealistic) representations of internal variability related to dynamics.

One goal of this research was to recommend better CMIP6 models for the three oceans adjacent to Canada. As we discussed above in this section, the North Atlantic Ocean and Arctic Ocean appear to have more predictability than the North Pacific Ocean. In general, the models' performance for the three oceans varies from one to another (Table 3.1), hence we would recommend using different models for each ocean when carrying out climate down-scaling at basin scales if possible, trying not to run one model including all the three oceans for climate projections. If the number of the down-scaling models needs to be smaller, we would suggest using one model to include both the North Atlantic Ocean and the Arctic Ocean, since the

dominant forcing mechanism related to the climate change is the same for them. UKESM1-0-LL, CNRM-ESM2-1 and CESM2 are the three models in the top 5 models for both the atmosphere component (SLP and AirT) and the ocean component (North Atlantic, Arctic and North Pacific), which underlines the importance of surface forcing (air temperature and wind) in the success of modelling oceans, as is commonly understood (Wang et al., 2015).

Acknowledgements:

This study is supported by the ESRF project “The performance and projections of the CMIP6 Earth System Models (ESMs) for Canada’s three oceans” (CC-22-05-01). DFO colleagues Li Zhai and Adam Drozdowski internally reviewed this report and provided helpful comments, which helped improve the quality of this report. The Head of the Ocean Modelling and Analysis Section, Mr. Andrew Cogswell, provided valuable assistance and management for the completion of the project – CC-22-05-10.

References

- Boden, T.A., Marland, G., and Andres, R. J. Global, Regional, and National Fossil-Fuel CO₂ Emissions (1751 - 2014) (V. 2017). United States: N. p., 1999. Web. doi:10.3334/CDIAC/00001_V2017.
- Crawford, A., Stroeve, J., Smith, A. et al. Arctic open-water periods are projected to lengthen dramatically by 2100. *Commun Earth Environ* 2, 109 (2021). <https://doi.org/10.1038/s43247-021-00183-x>
- Demory, M.-E., Berthou, S., Fernández, J., Sørland, S. L., Brogli, R., Roberts, M. J., Beyerle, U., Seddon, J., Haarsma, R., Schär, C., Buonomo, E., Christensen, O. B., Ciarlo, J. M., Fealy, R., Nikulin, G., Peano, D., Putrasahan, D., Roberts, C. D., Senan, R., Steger, C., Teichmann, C., and Vautard, R., 2020. European daily precipitation according to EURO-CORDEX regional climate models (RCMs) and high-resolution global climate models (GCMs) from the High-Resolution Model Intercomparison Project (HighResMIP). *Geosci. Model Dev.*, 13, 5485–5506, <https://doi.org/10.5194/gmd-13-5485-2020>.
- Enfield, D.B., A. M. Mestas-Nunez and P.J. Trimble, 2001. The Atlantic multidecadal oscillation and its relation to rainfall and river flows in the continental U.S.. *Geophysical Research Letters*, Vol. 28, 2077-2080, <https://doi.org/10.1029/2000GL012745>.
- GISTEMP Team, 2022. GISS Surface Temperature Analysis (GISTEMP), version 4. NASA Goddard Institute for Space Studies. <https://data.giss.nasa.gov/gistemp/>.
- Hamouda, M.E., Pasquero, C., and Tziperman, E., 2021. Decoupling of the Arctic Oscillation and North Atlantic Oscillation in a warmer climate. *Nat. Clim. Chang.* 11, 137–142, <https://doi.org/10.1038/s41558-020-00966-8>.
- Hurrell, J.W., 1995. Decadal trends in the North Atlantic Oscillation and relationships to regional temperature and precipitation. *Science* 269, 676-679, <https://doi.org/10.1126/science.269.5224.676>.
- Jones, P.D., Jónsson, T. and Wheeler, D., 1997. Extension to the North Atlantic Oscillation using early instrumental pressure observations from Gibraltar and South-West Iceland. *Int. J. Climatol.*

17, 1433-1450, [https://doi.org/10.1002/\(SICI\)1097-0088\(19971115\)17:13%3C1433::AID-JOC203%3E3.0.CO;2-P](https://doi.org/10.1002/(SICI)1097-0088(19971115)17:13%3C1433::AID-JOC203%3E3.0.CO;2-P).

Lenssen, N., G. Schmidt, J. Hansen, M. Menne, A. Persin, R. Ruedy, and D. Zyss, 2019. Improvements in the GISTEMP uncertainty model. *J. Geophys. Res. Atmos.*, 124, no. 12, 6307-6326, <https://doi.org/10.1029/2018JD029522>.

Loder, J.W. and Wang, Z. (2015) Trends and Variability of Sea Surface Temperature in the Northwest Atlantic from Three Historical Gridded Datasets, *Atmosphere-Ocean*, 53:5, 510-528, <https://doi.org/10.1080/07055900.2015.1071237>.

National Centers for Environmental Prediction/National Weather Service/NOAA/U.S. Department of Commerce, 1996. NCEP/NCAR Reanalysis Monthly Mean Subsets (from DS090.0), 1948-continuing. Research Data Archive at the National Center for Atmospheric Research, Computational and Information Systems Laboratory, Boulder, Colo., (Updated monthly). Accessed 2022-11-01. <https://doi.org/10.5065/4Z6T-J350>.

Notz, D., & SIMIP Community (2020). Arctic sea ice in CMIP6. *Geophysical Research Letters*, 47, e2019GL086749. <https://doi.org/10.1029/2019GL086749>

Rayner, N. A., Parker, D. E., Horton, E.B., Folland, C.K., Alexander, L.V., Rowell, D.P., Kent, E.C., Kaplan, A., 2003 Global analyses of sea surface temperature, sea ice, and night marine air temperature since the late nineteenth century, *J. Geophys. Res.* Vol. 108, No. D14, 4407, <https://doi.org/10.1029/2002JD002670>.

Reader, M.C., Steiner, N. Atmospheric trends over the Arctic Ocean in simulations from the Coordinated Regional Downscaling Experiment (CORDEX) and their driving GCMs. *Clim Dyn* 59, 3401–3426 (2022). <https://doi.org/10.1007/s00382-022-06274-5>

Shepherd, T. Atmospheric circulation as a source of uncertainty in climate change projections. *Nature Geosci* 7, 703–708 (2014). <https://doi.org/10.1038/ngeo2253>

Shu, Q., Wang, Q., Arthun, M., Wang, S., Song, Z., Zhang, M., and Qiao, F. (2022) ,Arctic Ocean Amplification in a warming climate in CMIP6 models. *Sci. Adv.* 8, eabn9755. DOI:10.1126/sciadv.abn9755

Smith, D.M., Scaife, A.A., Eade, R. et al. North Atlantic climate far more predictable than models imply. *Nature* 583, 796–800 (2020). <https://doi.org/10.1038/s41586-020-2525-0>

Trenberth, K.E. and Hurrell, J.W., 1994. Decadal atmosphere-ocean variations in the Pacific. *Clim. Dyn.*, 9, 303-319, <https://doi.org/10.1007/BF00204745>.

Walker, Gilbert T. and E.W. Bliss, 1932. "World weather V" (PDF). *Memoirs of the Royal Meteorological Society*. 4: 53–84, <https://www.rmets.org/sites/default/files/papers/ww5.pdf>

Wang, M., Overland, J. E., & Bond, N. A., 2010. Climate projections for selected large marine ecosystems. *Journal of Marine Systems*, 79(3-4), 258-266, <https://doi.org/10.1016/j.jmarsys.2008.11.028>.

Wang, M., Overland, J. E., and Stabeno, P., 2012. Future climate of the Bering and Chukchi Seas projected by global climate models. *Deep Sea Research Part II: Topical Studies in Oceanography*, 65, 46-57, <https://doi.org/10.1016/j.dsr2.2012.02.022>.

Wang, Z., Lu, Y., Dupont, F., Loder, J., Hannah, C. and Wright, D., 2015. Variability of sea surface height and circulation in the North Atlantic: Forcing mechanisms and linkages, *Progress in Oceanography*, 132, 273-286, <https://doi.org/10.1016/j.pocean.2013.11.004>.

Wang, Z., Brickman, D., Greenan, B., and Yashayaev, I., 2016. An abrupt shift in the Labrador Current System in relation to winter NAO events, *J. Geophys. Res. Oceans*, 121, 5338– 5349, <https://doi.org/10.1002/2016JC011721>.

Wang, Z., Hamilton, J., Su, J., 2017. Variations in freshwater pathways from the Arctic Ocean into the North Atlantic Ocean. *Progr. Oceanogr.*, 155, 54-73, <https://doi.org/10.1016/j.pocean.2017.05.012>.

Wang, Z., Brickman, D. and Greenan, B., 2019. Characteristic evolution of the Atlantic Meridional Overturning Circulation from 1990 to 2015: An eddy-resolving ocean model study. *Deep Sea Research Part I*, <https://doi.org/10.1016/j.dsr.2019.06.002>.

Zhou, S., A. J. Miller, J. Wang, and J. K. Angell, 2001. Trends of NAO and AO and their associations with stratospheric processes. *Geophys. Res. Lett.*, 28, 4107-4110, <https://doi.org/10.1029/2001GL013660>.

Tables

Table 2.2.1 Correlation coefficients (Cr) between NCEP PCs and CMIP6 PCs, and air temperature bias (Bias) between CMIP6 models and NCEP. Note: the confidence level of the correlation less than 95% is indicated by underlining the correlation coefficient.

Model	Sea level pressure			Air temperature (2m)		
	<i>Cr: PC1</i>	<i>Cr: PC2(JFM)</i>	<i>Cr: PC2</i>	<i>Cr: PC1</i>	<i>Cr: PC2</i>	<i>Bias</i>
ACCESS-CM2	<u>0.08</u>	<u>-0.03</u>	<u>-0.06</u>	0.86	<u>0.05</u>	-0.84
ACCESS-ESM1-5	<u>0.15</u>	<u>0.26</u>	<u>0.16</u>	0.91	<u>-0.01</u>	0.70
AWI-CM-1-1-MR	<u>0.09</u>	<u>0.08</u>	<u>0.19</u>	0.91	<u>0.02</u>	1.08
CAMS-CSM1-0	<u>0.16</u>	<u>0.06</u>	<u>0.19</u>	0.71	<u>0.03</u>	-0.79
CanESM5	<u>-0.15</u>	<u>-0.06</u>	<u>-0.01</u>	0.89	-0.46	-0.06
CESM2	<u>0.14</u>	<u>0.05</u>	<u>0.15</u>	0.86	<u>0.12</u>	1.34
CESM2-WACCM	<u>-0.04</u>	<u>-0.01</u>	<u>-0.01</u>	0.87	<u>-0.18</u>	0.95
CMCC-CM2-SR5	<u>0.00</u>	<u>0.02</u>	-0.25	0.86	-0.28	2.16
CNRM-CM6-1	0.29	<u>-0.10</u>	<u>0.08</u>	0.80	<u>0.06</u>	-0.66
CNRM-CM6-1-HR	<u>-0.16</u>	<u>0.00</u>	<u>0.11</u>	0.89	<u>-0.17</u>	-1.08
CNRM-ESM2-1	0.25	<u>0.09</u>	<u>0.13</u>	0.85	<u>0.13</u>	0.09
EC-Earth3	<u>0.12</u>	<u>0.09</u>	<u>0.01</u>	0.92	<u>-0.10</u>	-0.84
GISS-E2-1-G	<u>0.02</u>	<u>0.01</u>	<u>0.08</u>	0.29	<u>0.00</u>	-1.12
IPSL-CM6A-LR	<u>-0.14</u>	-0.23	<u>-0.20</u>	0.89	<u>-0.11</u>	0.24
MIROC6	<u>0.02</u>	<u>0.02</u>	<u>0.04</u>	0.67	-0.28	1.44
MIROC-ES2L	<u>0.02</u>	<u>-0.08</u>	<u>0.10</u>	0.64	<u>0.04</u>	0.78
MPI-ESM1-2-HR	<u>-0.05</u>	0.29	0.42	0.79	<u>0.15</u>	0.83
MPI-ESM1-2-LR	<u>0.15</u>	<u>0.05</u>	<u>-0.01</u>	0.89	<u>-0.07</u>	0.34
MRI-ESM2-0	<u>0.01</u>	<u>-0.04</u>	<u>0.02</u>	0.80	-0.18	1.04
NorESM2-LM	<u>-0.02</u>	<u>-0.11</u>	<u>0.13</u>	0.84	<u>-0.12</u>	0.95
TaiESM1	<u>-0.19</u>	<u>-0.03</u>	<u>-0.03</u>	0.88	<u>0.01</u>	-0.39
UKESM1-0-LL	<u>0.16</u>	0.25	0.27	0.85	0.33	-1.30

Table 2.3.1 Correlation coefficients (Cr) between HadISST PCs and CMIP6 PCs for the North Atlantic Ocean and North Pacific Ocean (SST), and SST bias (Bias) between CMIP6 models and HadISST for the two oceans. Note: the confidence level of the correlation less than 95% is indicated by underlining the correlation coefficient.

Model	North Atlantic Ocean			North Pacific Ocean		
	<i>Cr: PC1</i>	<i>Cr: PC2</i>	<i>Bias</i>	<i>Cr: PC1</i>	<i>Cr: PC2</i>	<i>Bias</i>
ACCESS-CM2	0.48	<u>-0.02</u>	-0.70	0.27	0.44	-1.45
ACCESS-ESM1-5	0.81	<u>-0.05</u>	0.22	<u>-0.04</u>	0.58	0.44
AWI-CM-1-1-MR	0.80	<u>0.22</u>	-0.38	0.28	0.73	-0.47
CAMS-CSM1-0	0.35	<u>0.17</u>	-1.71	<u>-0.09</u>	0.55	-1.11
CanESM5	0.74	<u>0.16</u>	-1.35	<u>-0.19</u>	0.61	-0.45
CESM2	0.76	<u>0.19</u>	0.77	<u>0.25</u>	0.65	0.24
CESM2-WACCM	0.78	<u>0.17</u>	0.67	<u>-0.10</u>	0.58	0.12
CMCC-CM2-SR5	0.68	<u>-0.03</u>	-0.07	<u>0.07</u>	0.63	0.37
CNRM-CM6-1	0.58	<u>0.09</u>	-0.66	<u>0.06</u>	0.70	-0.13
CNRM-CM6-1-HR	0.67	<u>-0.01</u>	-1.36	<u>0.06</u>	0.58	-0.54
CNRM-ESM2-1	0.68	0.31	-0.15	<u>0.14</u>	0.70	0.45
EC-Earth3	0.84	<u>-0.12</u>	-1.19	0.44	0.78	-0.16
GISS-E2-1-G	0.77	<u>-0.09</u>	-0.50	<u>0.15</u>	0.37	-1.78
IPSL-CM6A-LR	0.31	<u>0.00</u>	-0.76	<u>-0.11</u>	0.60	-0.12
MIROC6	0.75	<u>0.18</u>	-0.78	<u>-0.03</u>	0.48	-0.86
MIROC-ES2L	0.64	<u>0.11</u>	-1.36	<u>0.10</u>	0.59	-1.10
MPI-ESM1-2-HR	0.59	<u>-0.14</u>	-0.75	<u>0.16</u>	0.59	-0.96
MPI-ESM1-2-LR	0.85	<u>-0.19</u>	-1.04	<u>0.02</u>	0.59	-1.37
MRI-ESM2-0	0.62	-0.41	-0.48	<u>0.02</u>	0.70	-0.35
NorESM2-LM	0.79	<u>-0.10</u>	0.44	<u>-0.08</u>	0.61	-0.46
TaiESM1	0.77	<u>-0.07</u>	0.24	-0.32	0.72	-0.54
UKESM1-0-LL	0.89	<u>0.23</u>	-1.10	<u>-0.15</u>	0.81	-0.97

Table 2.3.2 Correlation coefficients (Cor. Coef.) between HadISST ice area and those of CMIP6 models for winter and summer (ice area), ice area bias (Bias) between modelled ice areas and HadISST, ice area trends(Trend) from HadISST(HD) and CMIP6 models, and the ratios (Ratio) between summer ice area trend and winter ice area trend.

Model	Cor. Coef.: winter	Cor. Coef.: summer	Bias: winter (10 ⁶ km ²)	Trend: winter HD (-14.3/yr) (10 ³ km ²)	Bias: summer (10 ⁶ km ²)	Trend: summer HD (-53.7/yr)(10 ³ km ²)	Ratio: (summer/sinter) HD (3.8)
ACCESS-CM2	<u>-0.04</u>	0.62	6.14	-1.1	0.53	-25.6	22.8
ACCESS-ESM1-5	0.48	0.75	4.84	-28.3	-0.31	-39.3	1.4
AWI-CM-1-1-MR	0.55	0.81	6.40	-23.9	-1.58	-36.3	1.5
CAMS-CSM1-0	<u>-0.20</u>	0.54	10.15	1.7	2.21	-18.1	-10.9
CanESM5	<u>0.24</u>	0.76	6.59	-15.0	1.57	-49.6	3.9
CESM2	0.51	0.86	5.20	-16.0	-1.37	-76.6	4.9
CESM2-WACCM	0.23	0.83	5.68	-11.1	0.22	-62.6	5.6
CMCC-CM2-SR5	0.45	0.57	3.74	-25.0	-5.68	-2.4	0.1
CNRM-CM6-1	0.55	0.69	5.75	-18.4	-0.19	-45.2	2.5
CNRM-ESM2-1	0.70	0.74	5.73	-25.8	-1.05	-39.5	1.5
EC-Earth3	0.64	0.88	6.70	-65.3	2.24	-86.6	1.3
GISS-E2-1-G	<u>0.17</u>	0.55	4.16	-5.3	2.86	-17.7	3.3
IPSL-CM6A-LR	<u>0.24</u>	0.86	5.52	-3.0	-0.82	-57.4	19.4
MIROC6	0.44	0.67	3.50	-14.5	-0.14	-21.1	1.5
MIROC-ES2L	0.48	0.54	4.22	-13.4	-0.90	-15.7	1.2
MPI-ESM1-2-HR	<u>0.12</u>	0.85	5.32	-5.4	-1.55	-37.1	6.9
MPI-ESM1-2-LR	0.51	0.83	4.66	-19.1	-1.08	-36.3	1.9
MRI-ESM2-0	<u>0.14</u>	0.70	7.13	-10.8	-0.41	-49.0	4.5
NorESM2-LM	0.60	0.74	5.59	-19.0	0.41	-34.4	1.8
TaiESM1	0.29	0.80	5.03	-9.6	1.08	-53.0	5.5
UKESM1-0-LL	0.64	0.75	6.43	-31.3	2.35	-49.5	1.6

Table 3.1 Model rankings for the three oceans

Model	North Atlantic Ocean (SST)	North Pacific Ocean (SST)	Arctic Ocean (ice area summer trend)	Averaged Ranking score
ACCESS-CM2	20	13	15	16
ACCESS-ESM1-5	8	15	9	10.7
AWI-CM-1-1-MR	2	2	12	5.3
CAMS-CSM1-0	18	20	18	18.7
CanESM5	7	19	3	9.7
CESM2	5	3	14	7.3
CESM2-WACCM	4	18	7	9.7
CMCC-CM2-SR5	17	9	21	15.7
CNRM-CM6-1	16	5	6	9
CNRM-CM6-1-HR	15	11		13
CNRM-ESM2-1	3	4	8	5
EC-Earth3	10	1	17	9.3
GISS-E2-1-G	13	22	19	18
IPSL-CM6A-LR	21	16	2	13
MIROC6	6	21	16	14.3
MIROC-ES2L	9	10	20	13
MPI-ESM1-2-HR	19	8	10	12.3
MPI-ESM1-2-LR	14	12	11	12.3
MRI-ESM2-0	22	7	5	11.3
NorESM2-LM	12	14	13	13
TaiESM1	11	17	1	9.7
UKESM1-0-LL	1	6	4	3.7

Table 4.1 Correlation coefficients for the EOFs.

Model	Atmosphere				Ocean			
	SLP		AirT		Atlantic		Pacific	
	EOF1	EOF2	EOF1	EOF2	EOF1	EOF2	EOF1	EOF2
ACCESS-CM2	0.82	0.95	0.21	0.58	0.58	0.28	0.54	0.11
ACCESS-ESM1-5	0.82	0.96	0.28	0.00	0.68	0.39	0.50	0.18
AWI-CM1-1-MR	0.82	0.93	0.30	0.10	0.35	0.71	0.80	0.64
CAMS-CSM1-0	0.84	0.92	0.13	0.21	0.03	-0.29	0.70	0.55
CanESM5	0.79	0.83	0.40	0.31	0.65	0.11	0.72	0.73
CESM2	0.88	0.94	0.40	0.32	0.73	0.80	0.82	0.63
CESM2-WACCM	0.88	0.98	0.40	0.43	0.73	0.57	0.80	0.64
CMCC-CM2-SR5	0.88	0.85	0.42	0.36	0.34	0.38	0.84	0.66
CNRM-CM6-1	0.84	0.94	0.56	0.74	0.72	0.55	0.74	0.57
CNRM-CM6-1-HR	0.86	0.96	0.36	0.68	0.53	0.63	0.74	0.62
CNRM-ESM2-1	0.83	0.91	0.57	0.76	0.69	0.71	0.52	0.71
EC-Earth3	0.89	0.93	0.38	0.51	0.65	0.62	0.80	0.65
GISS-E2-1-G	0.81	0.85	0.02	0.39	0.05	0.61	0.64	0.55
IPSL-CM6A-LR	0.82	0.92	0.46	0.69	0.70	0.48	0.75	0.37
MIROC6	0.85	0.93	0.19	0.03	0.71	0.67	0.83	0.32
MIROC-ES2L	0.77	0.88	0.09	0.09	0.62	0.13	0.64	0.31
MPI-ESM1-2-HR	0.84	0.89	0.21	0.66	0.15	0.55	-0.30	0.60
MPI-ESM1-2-LR	0.82	0.90	0.34	0.52	0.53	0.65	0.77	0.63
MRI-ESM2-0	0.91	0.95	0.57	0.70	-0.07	0.33	0.72	0.35
NorESM2-LM	0.86	0.92	0.27	0.62	0.53	0.58	0.64	0.27
TaiESM1	0.88	0.90	0.44	0.59	0.33	0.55	0.80	0.64
UKESM1-0-LL	0.80	0.97	0.46	0.68	0.74	0.56	0.76	0.71

Figures

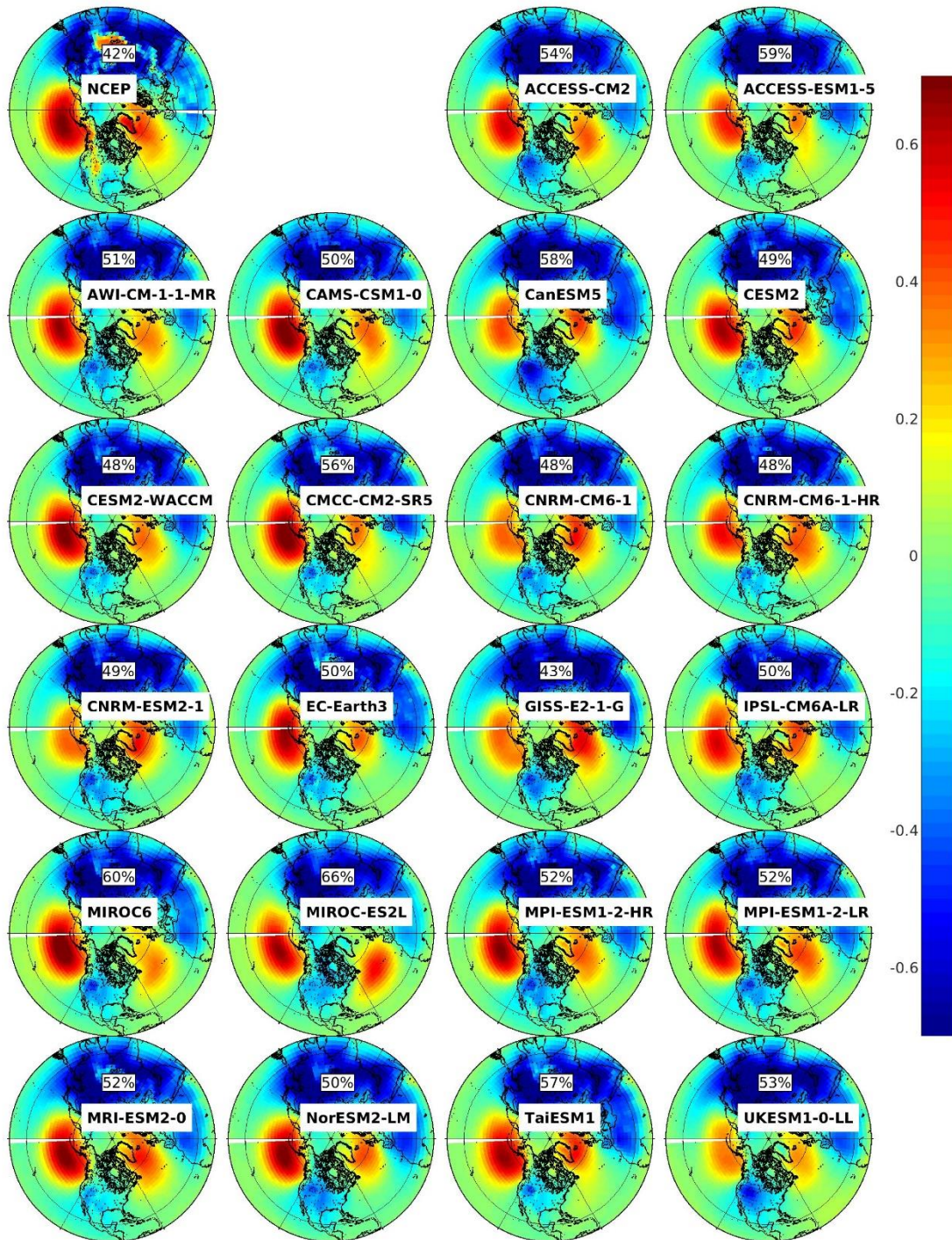


Figure 2.2.1. EOF1 patterns of the CMIP6 ESMs and NCEP for sea level pressure. The percentage of variance accounted for by EOF1 is indicated.

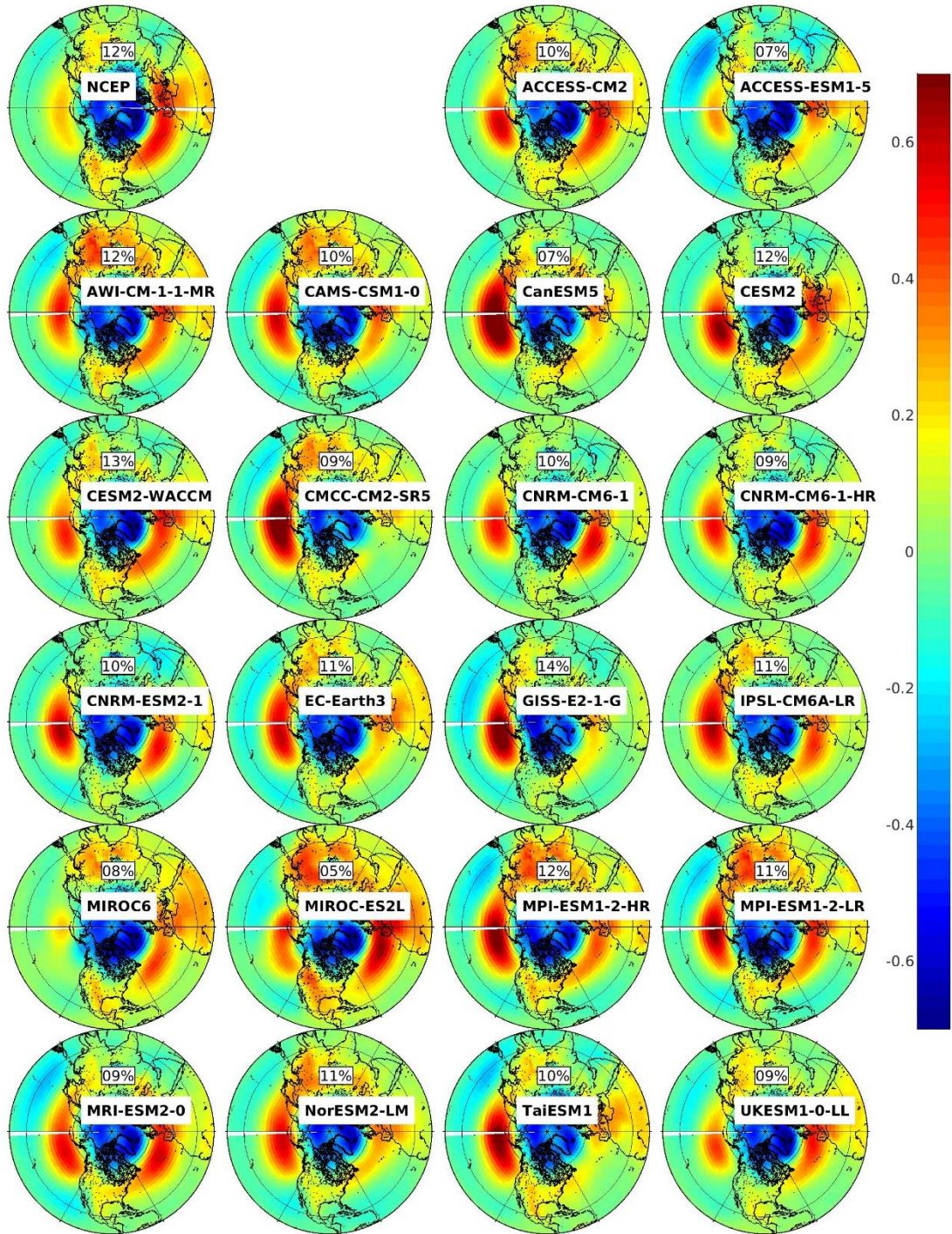


Figure 2.2.2. EOF2 patterns of the CMIP6 ESMs and NCEP for sea level pressure. The percentage of variance accounted for by EOF2 is indicated.

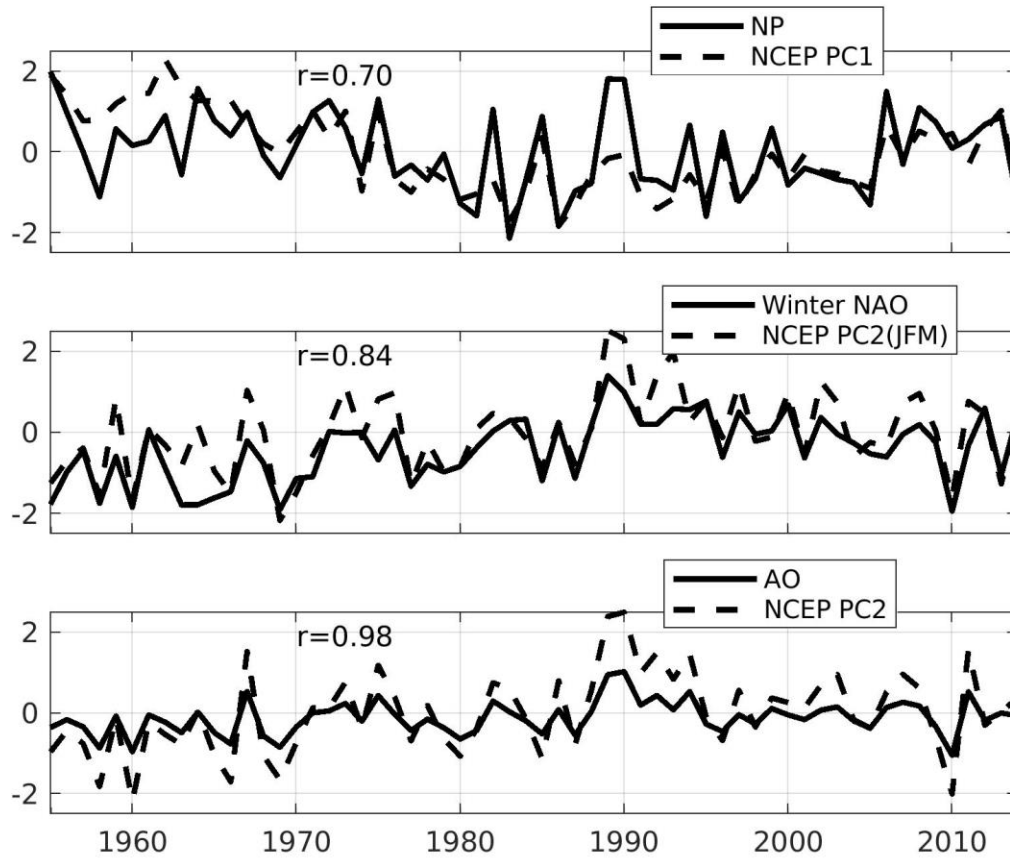


Figure 2.2.3. Time series of the NCEP PCs (SLP; annual mean PC1: top; PC2(JFM): middle; annual mean PC2: bottom) and atmospheric indices, NP, Winter NAO, and AO. Note: prior to plotting, for each quantity, the mean over the whole period was removed, and each quantity was normalized with its standard deviation.

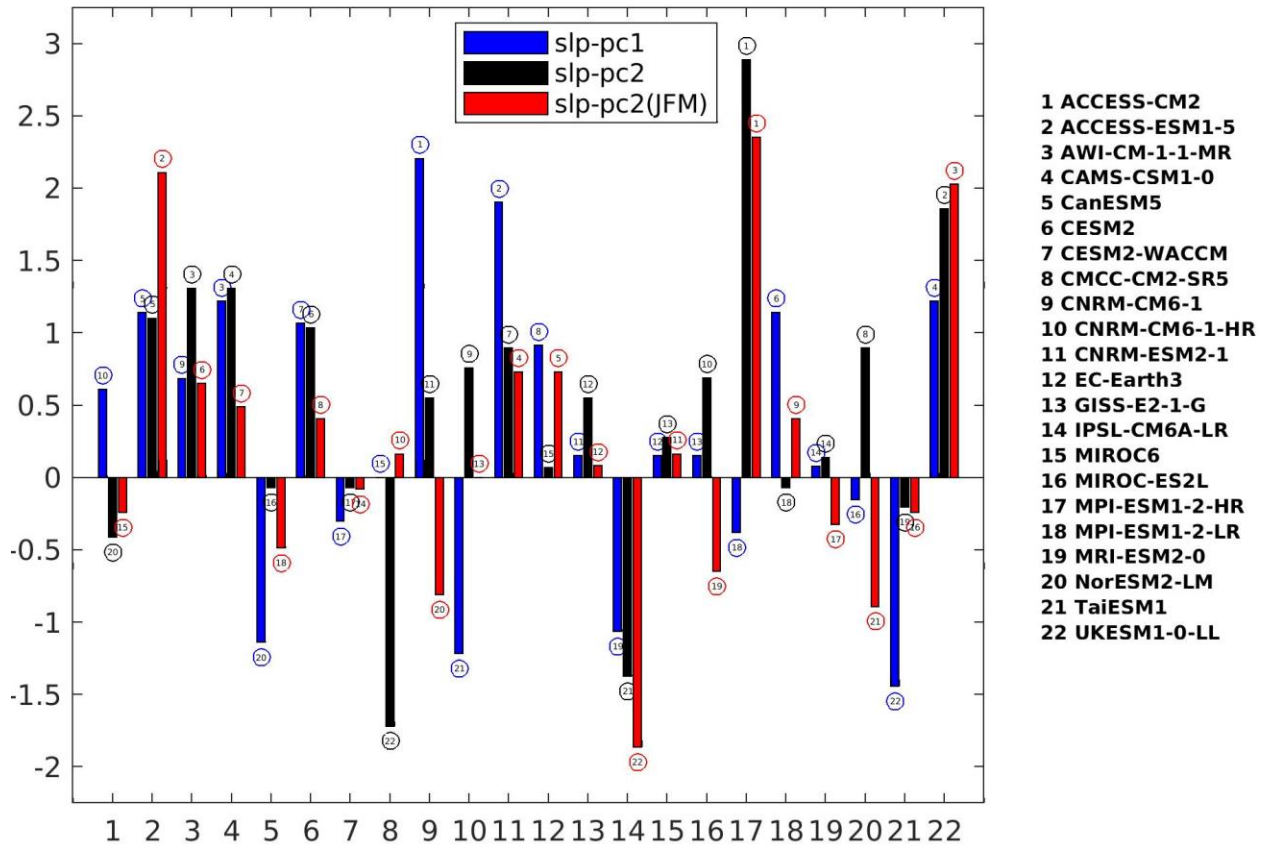


Figure 2.2.4. Performance score based on correlation coefficients. The circled number is the model rank. CMIP6 model is indicated by the number on x-axis.

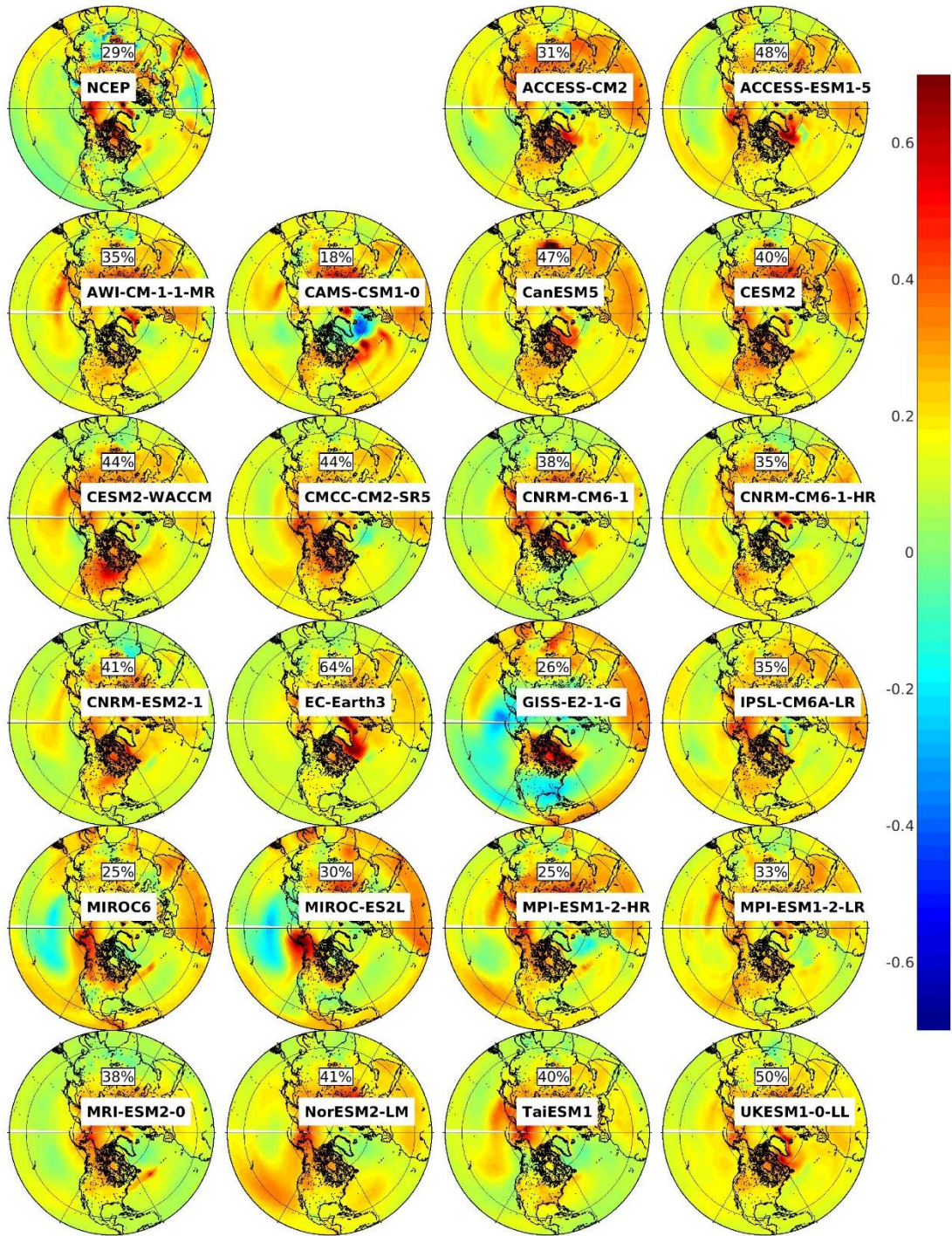


Figure 2.2.5. EOF1 patterns of the CMIP6 ESMs and that of NCEP for the air temperature at 2m above earth surface. The percentage of variance accounted for by EOF1 is indicated.

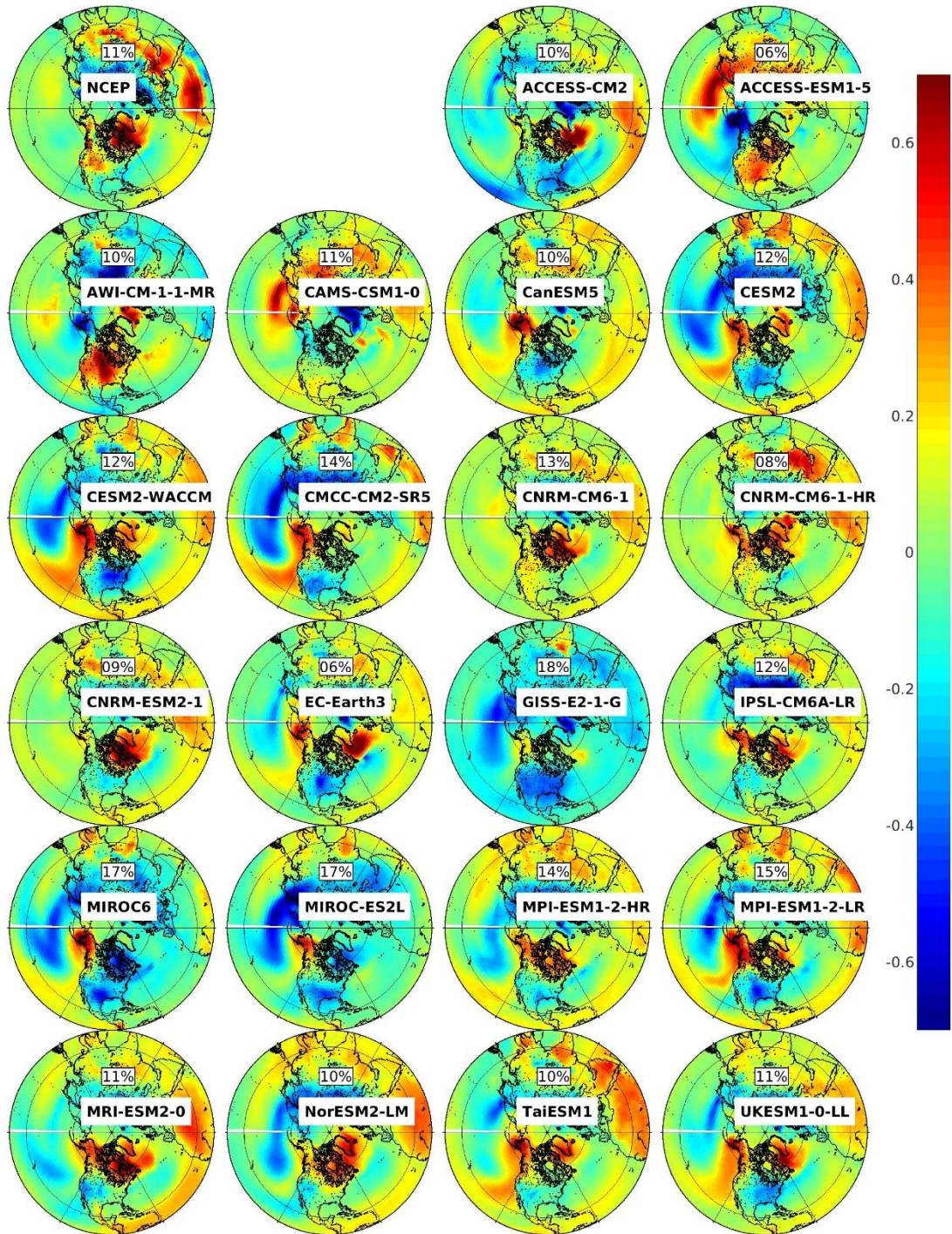


Figure 2.2.6. EOF2 patterns of the CMIP6 ESMs and that of NCEP for the air temperature at 2m above earth surface. The percentage of variance accounted for by EOF2 is indicated.

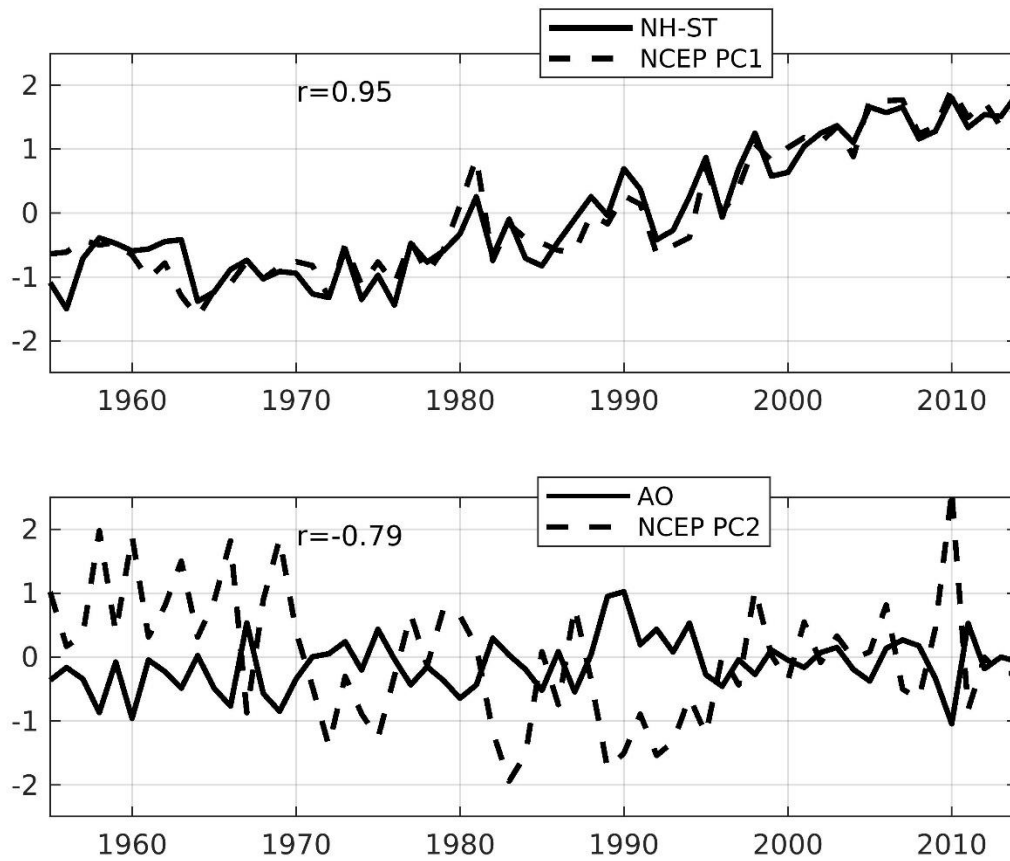


Figure 2.2.7. Time series of NCEP annual mean 2m air temperature AirT PC1 (top) and PC2 (bottom) and atmospheric indices, northern hemisphere land-ocean temperature index(NH-ST) and Arctic Oscillation(AO).

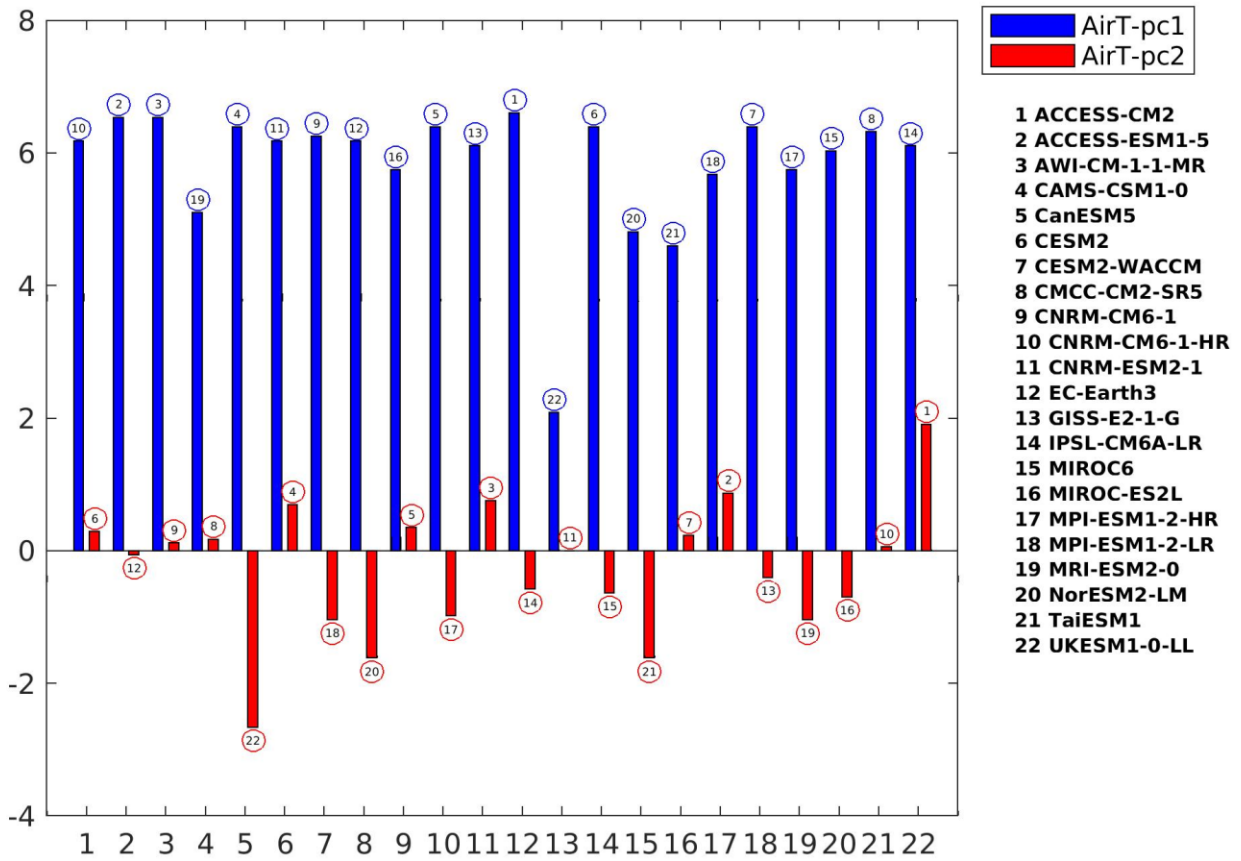


Figure 2.2.8. Performance score based on correlation coefficients (NCEP and CMIP6). The circled number is the model rank. CMIP6 model is indicated by the number on x-axis.

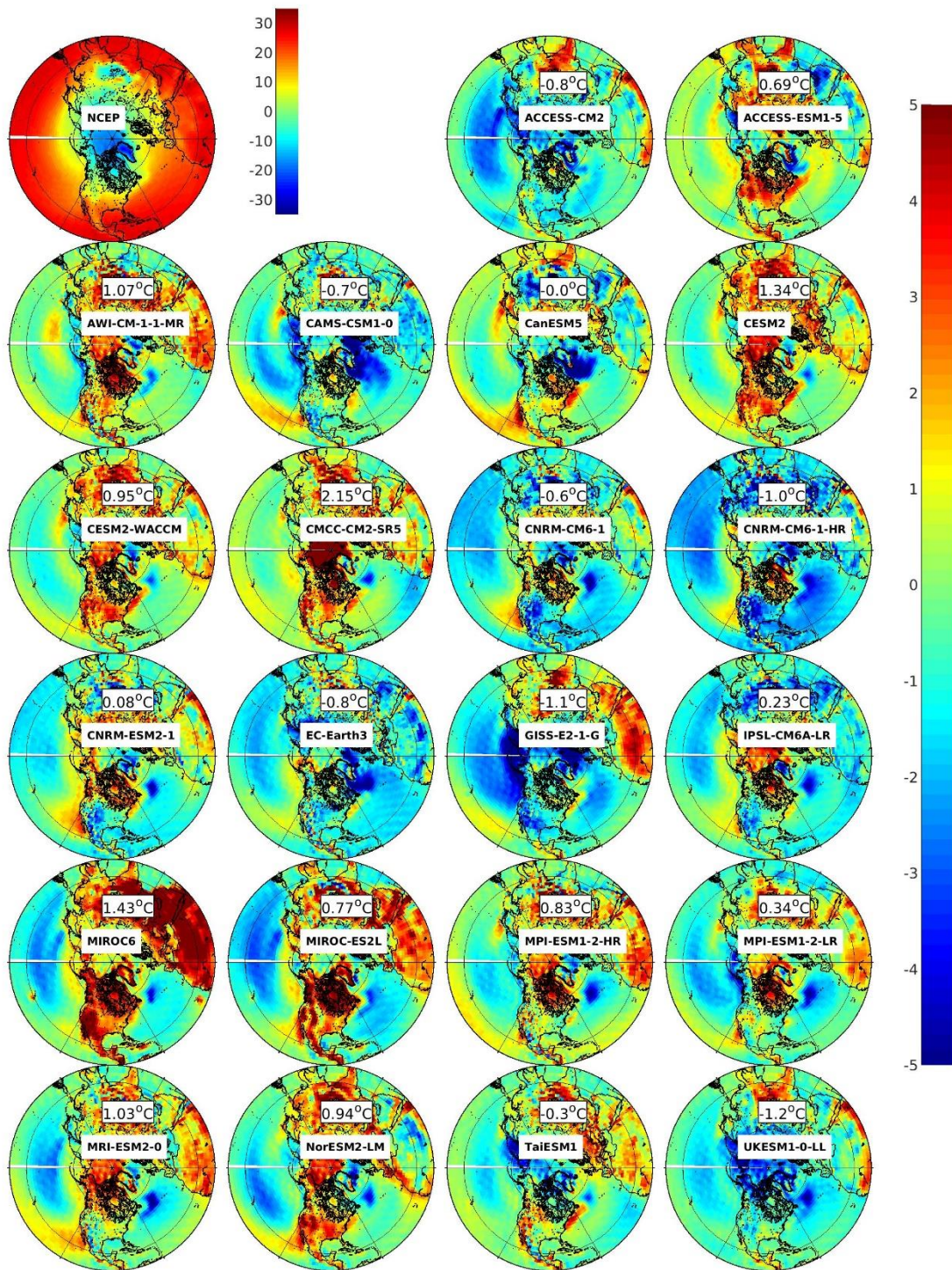


Figure 2.2.9. 60-year mean 2m air temperature from NCEP, and the differences between 60-year mean air temperatures of CMIP6 ESMs and NCEP.

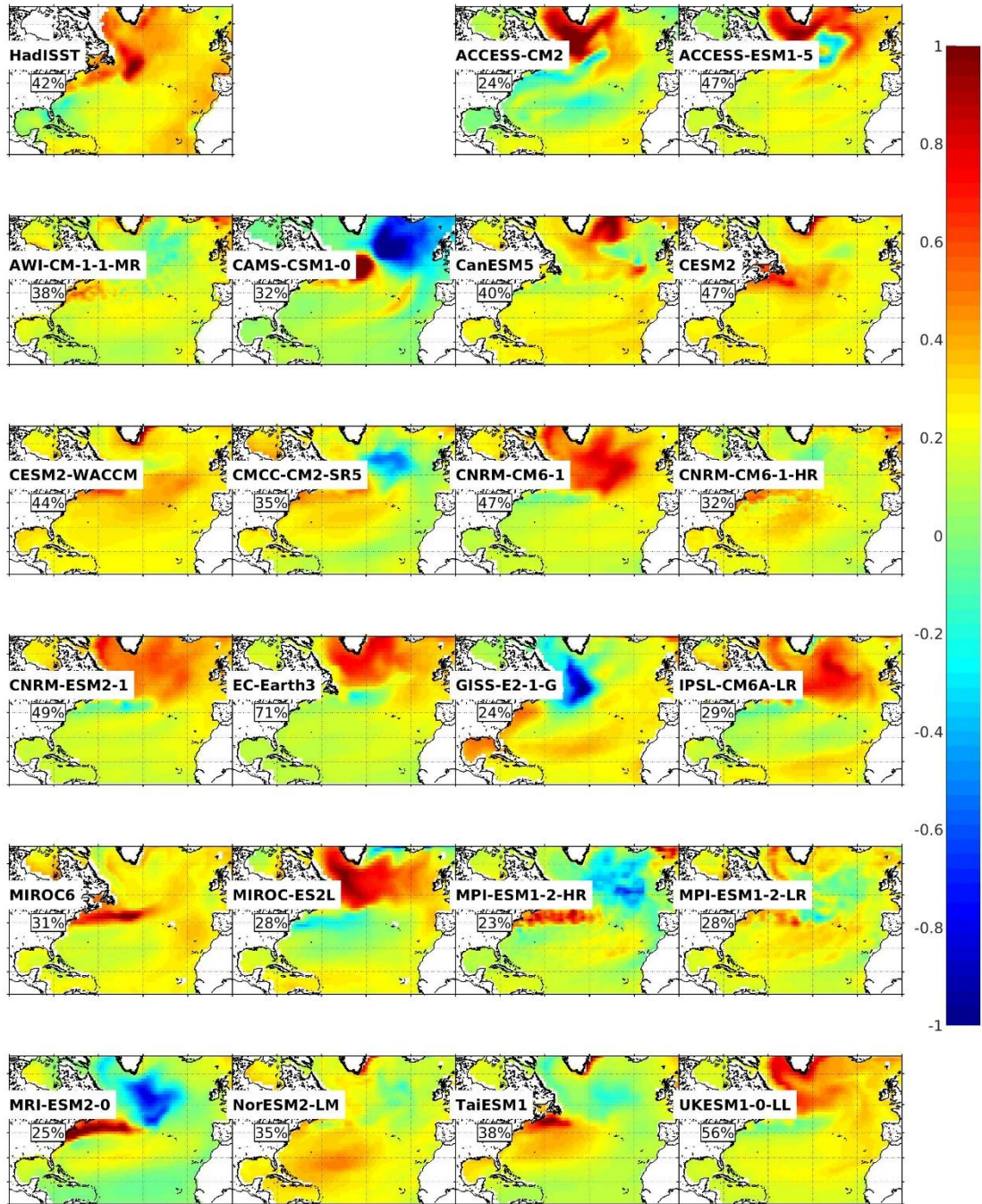


Figure 2.3.1. EOF1 patterns of the CMIP6 ESMs and that HadISST for SST

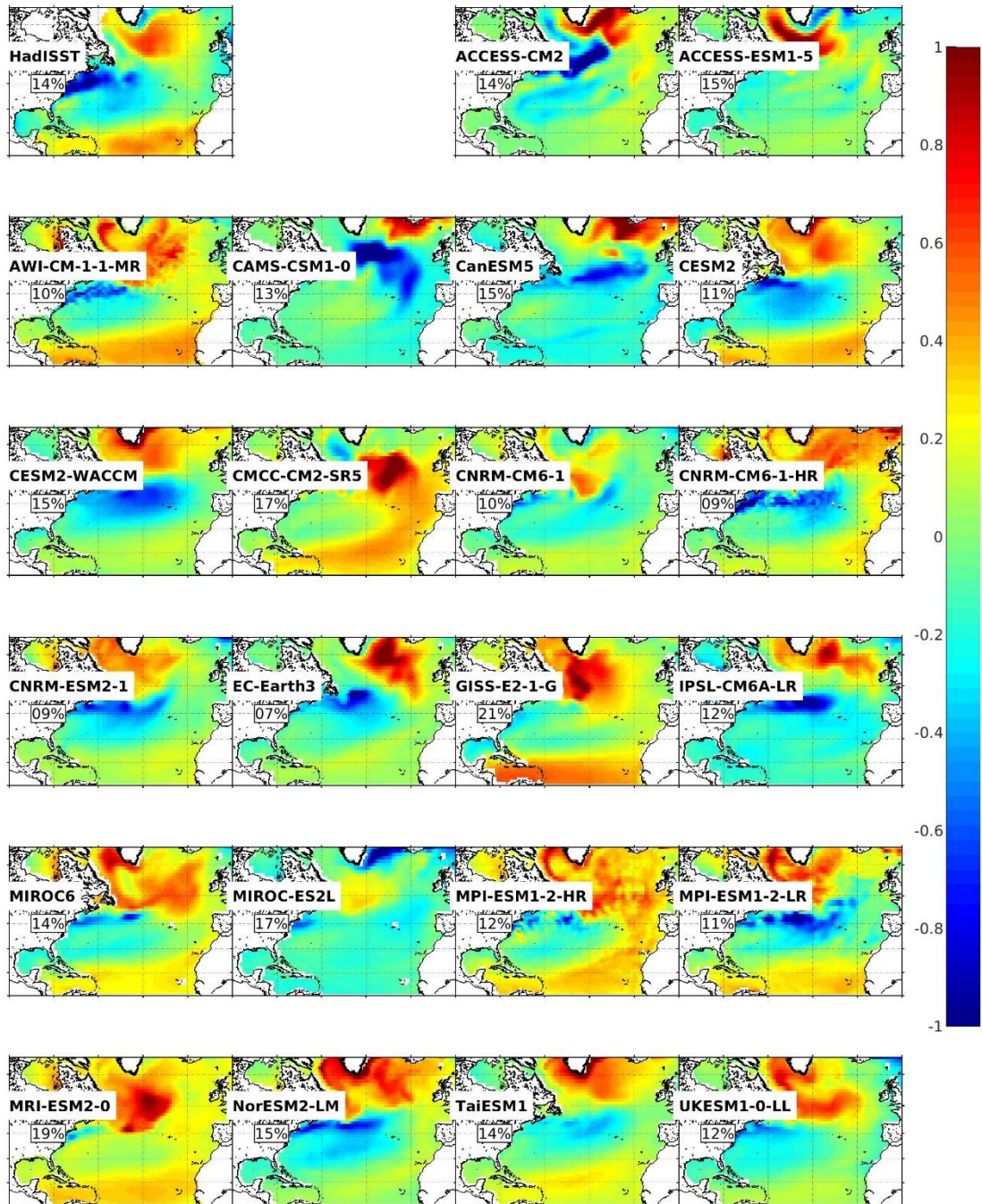


Figure 2.3.2. EOF2 patterns of the CMIP6 ESMs and that HadISST for SST

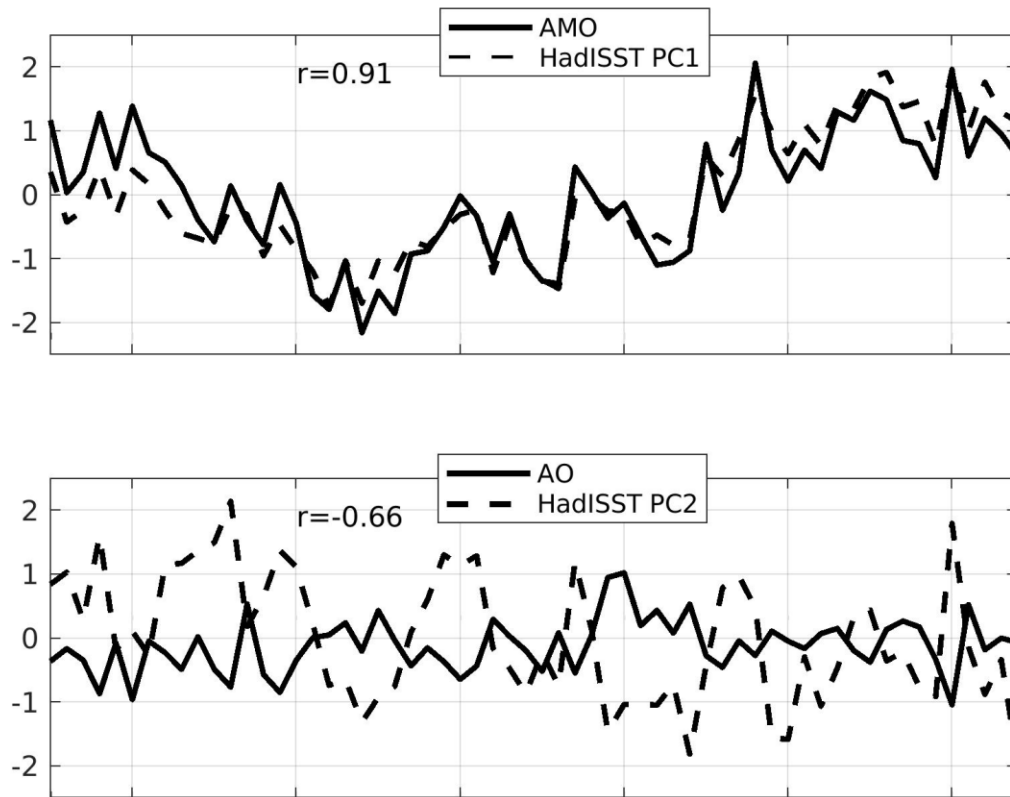


Figure 2.3.3. Time series of HadISST PC1 (top) and PC2 (bottom) and AMO and AO.

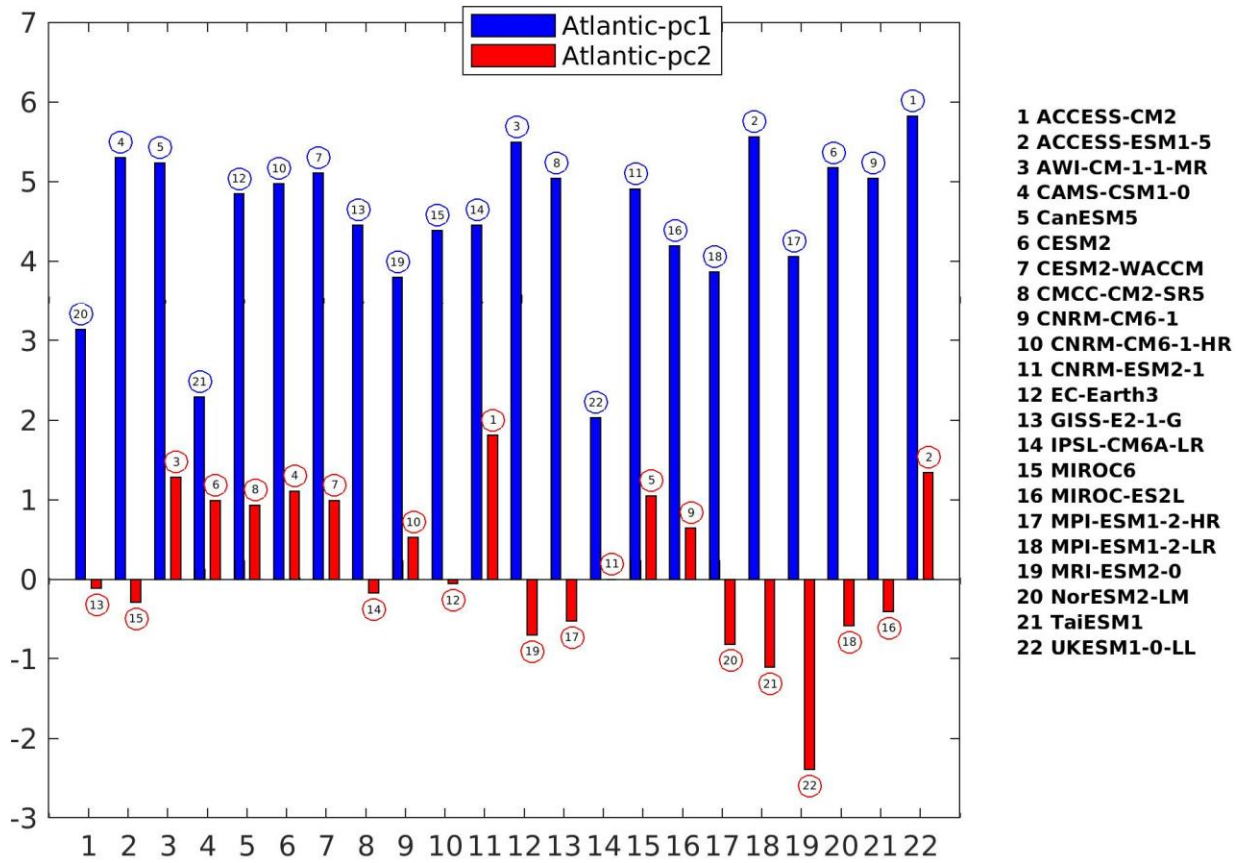


Figure 2.3.4. Performance score based on correlation coefficients (HadISST and CMIP6). The circled number is the model rank. CMIP6 model is indicated by the number on x-axis.

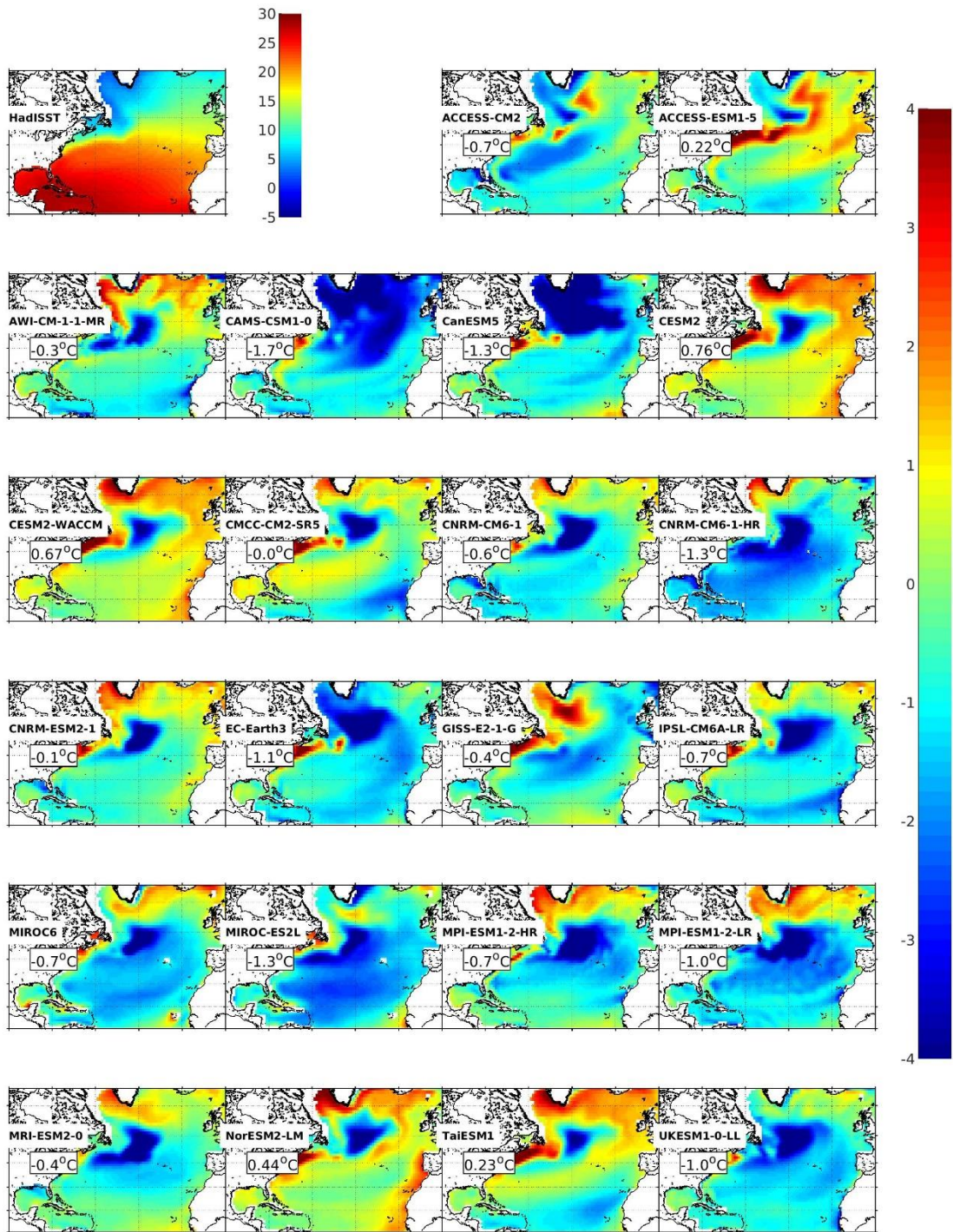


Figure 2.3.5 60-year mean SST from HadISST, and the differences between 60-year mean SST of CMIP6 ESMs and HadISST.

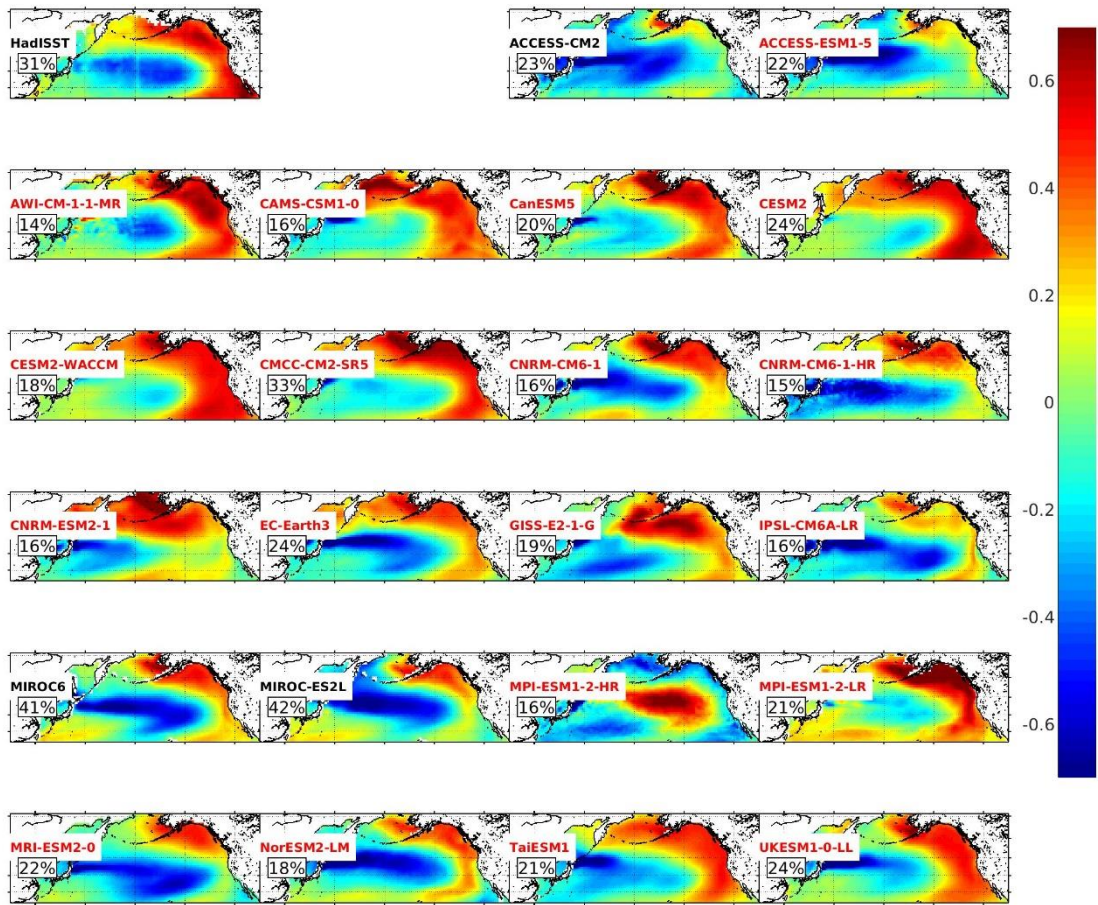


Figure 2.3.6. EOF1 patterns of the CMIP6 ESMs and that HadISST for SST. Model names are indicated in red, the pattern is from original EOF2.

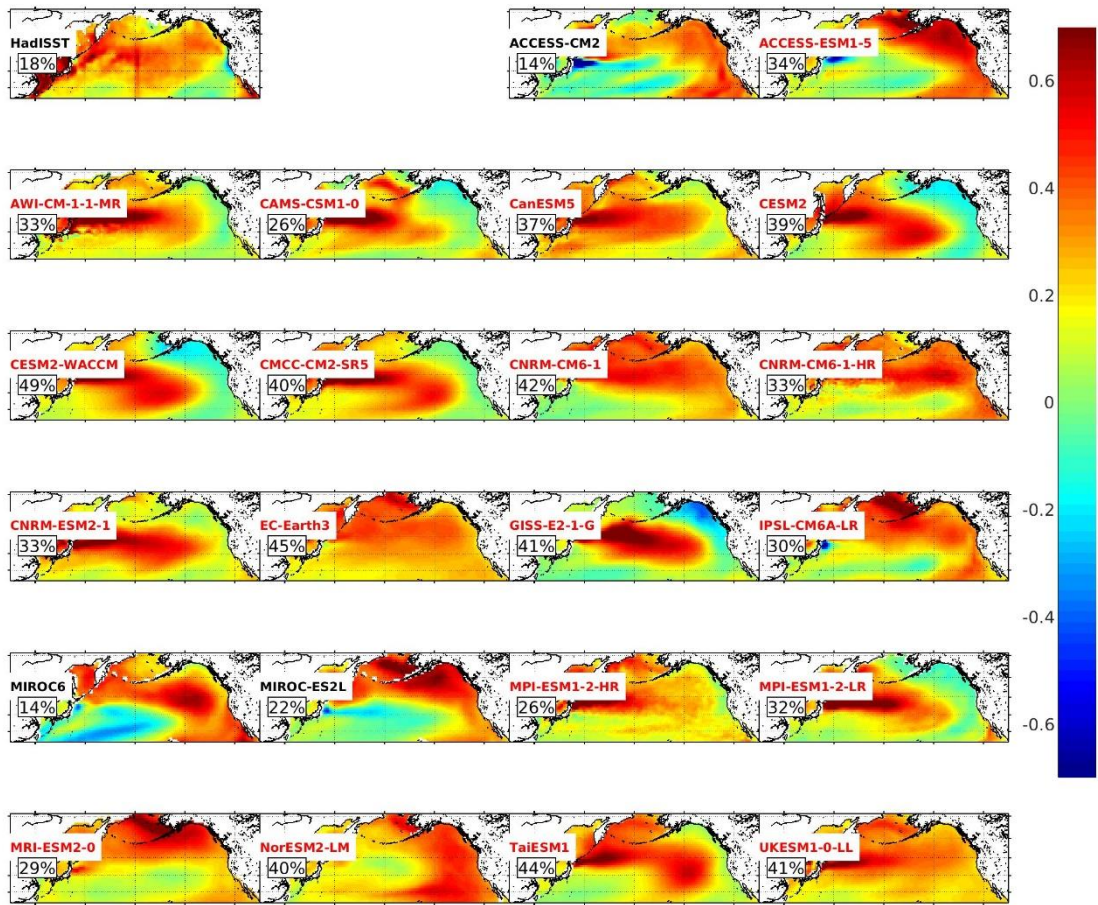


Figure 2.3.7. EOF2 patterns of the CMIP6 ESMs and that HadISST for the SST. For the model's name in red, the pattern is from original EOF1.

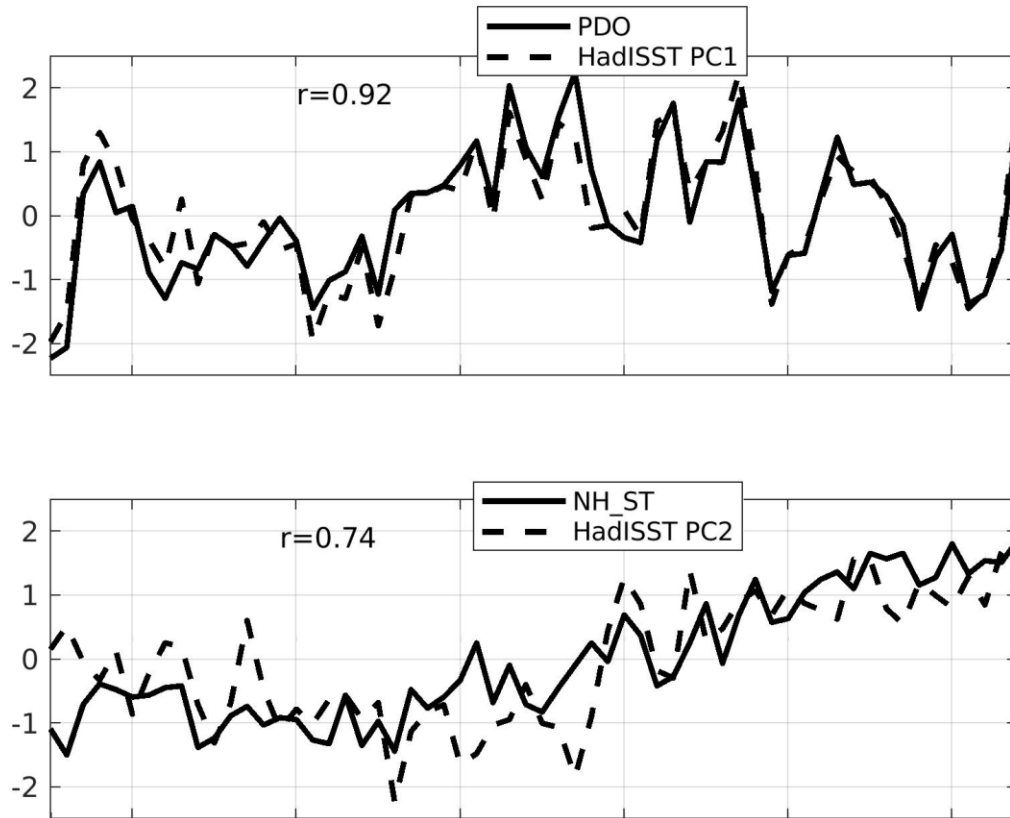


Figure 2.3.8 Time series of HadISST PC1 (top) and PC2 (bottom) and PDO and NH-ST.

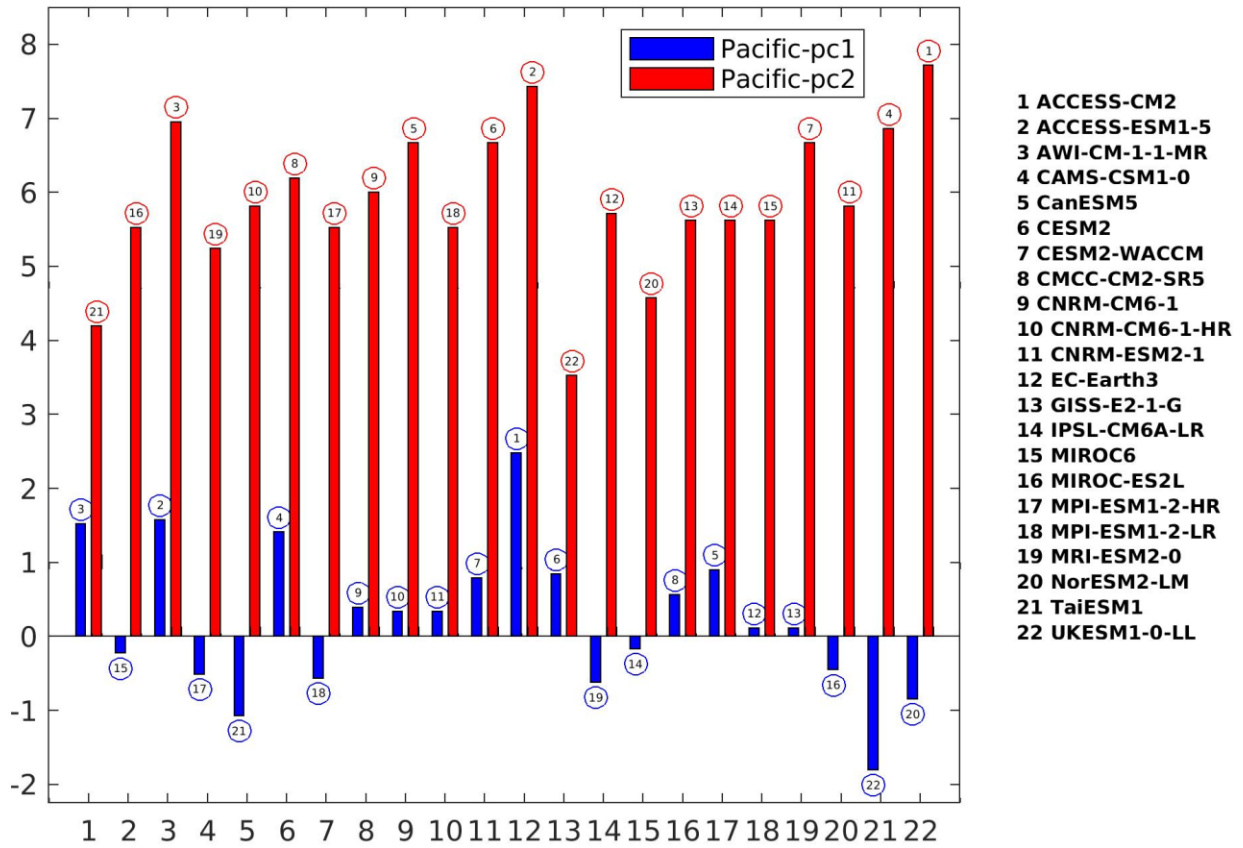


Figure 2.3.9. Performance score based on correlation coefficients (HadISST and CMIP6). The circled number is the model rank. The CMIP6 model is indicated by the number on x-axis . Note: The majority of the CMIP6 ESMs have their PC1 and PC2 switched (indicated in their EOFs' patterns).

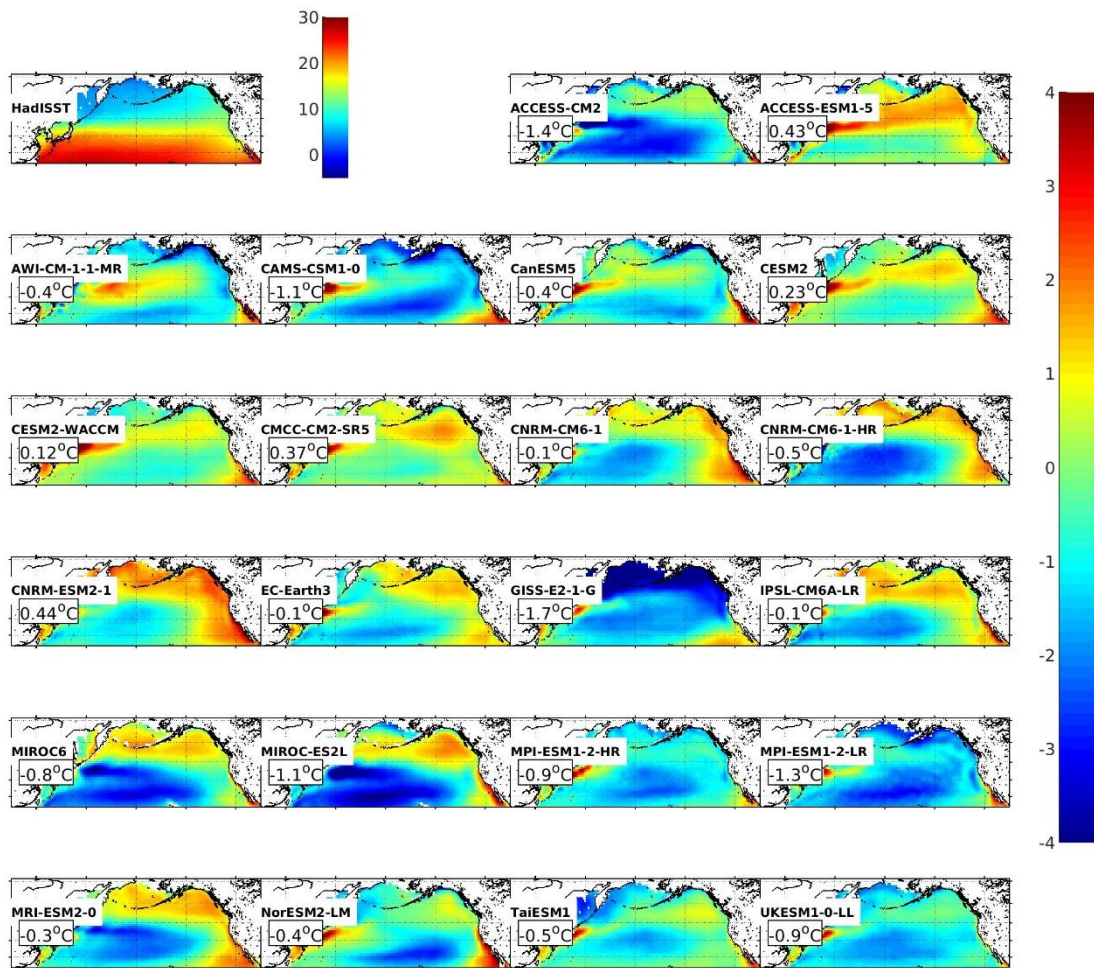


Figure 2.3.10. 60-year mean SST from HadISST, and the differences between 60-year mean SST of CMIP6 ESMs and HadISST.

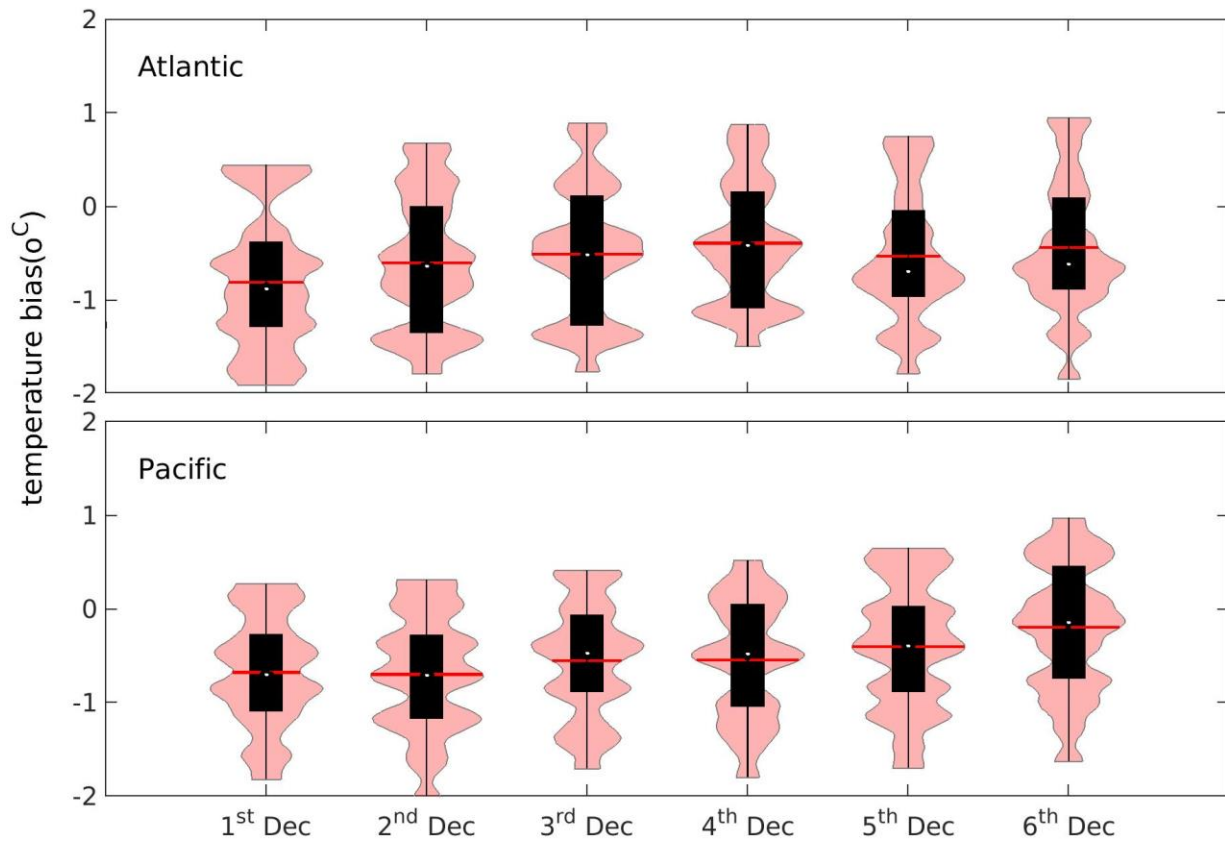


Figure 2.3.11. Violin plots of decadal mean biases for the North Atlantic Ocean and North Pacific Ocean. The boxes indicate the interquartile range (IQR), and whiskers are 1.5 IQR. Horizontal line is for mean value, and white circle is for median value. The six decades are indicated on the x-axis for the 1955 to 2014 period.

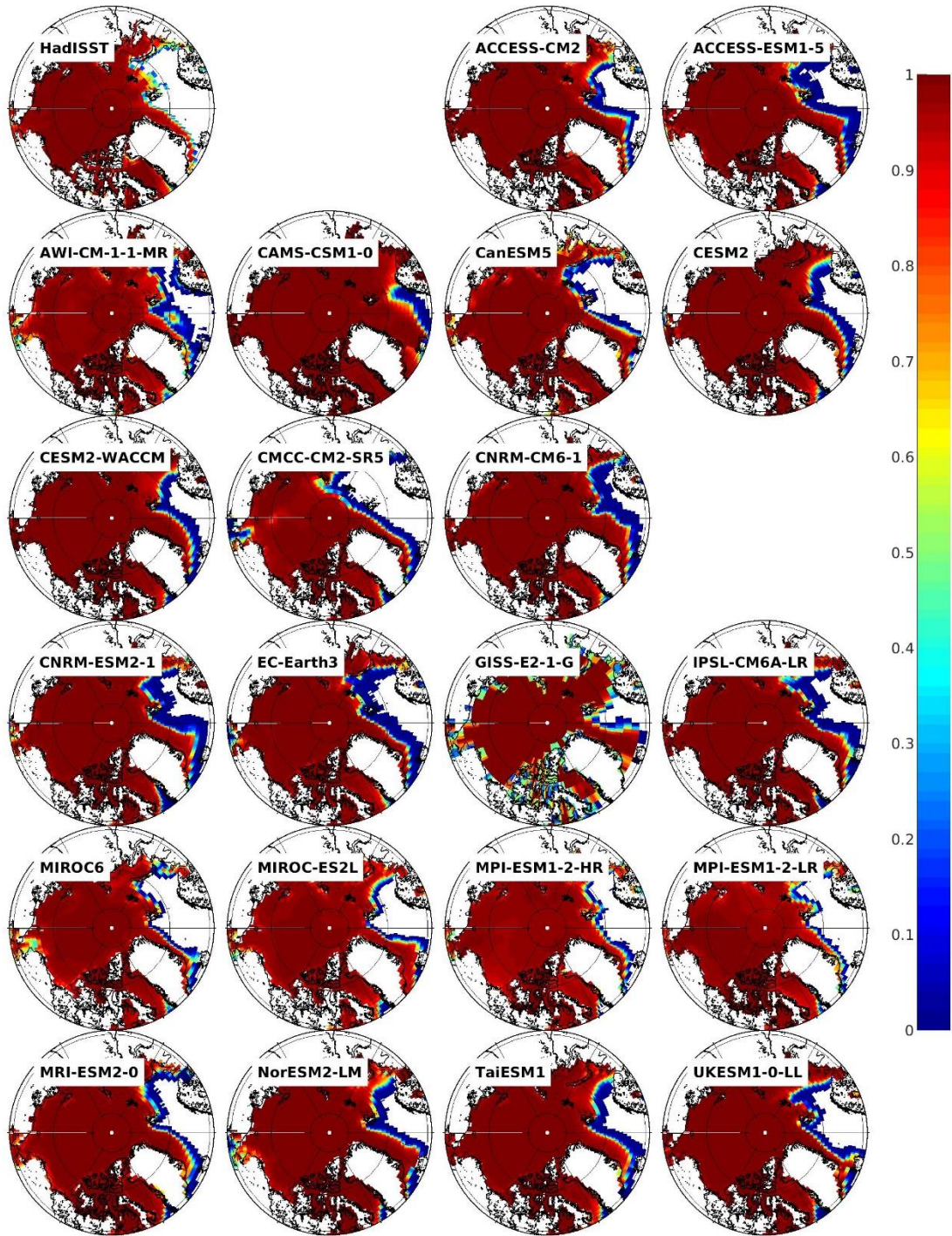


Figure 2.3.12. Sea ice concentration in March of 2014 from HadISST and CMIP6 ESMs.

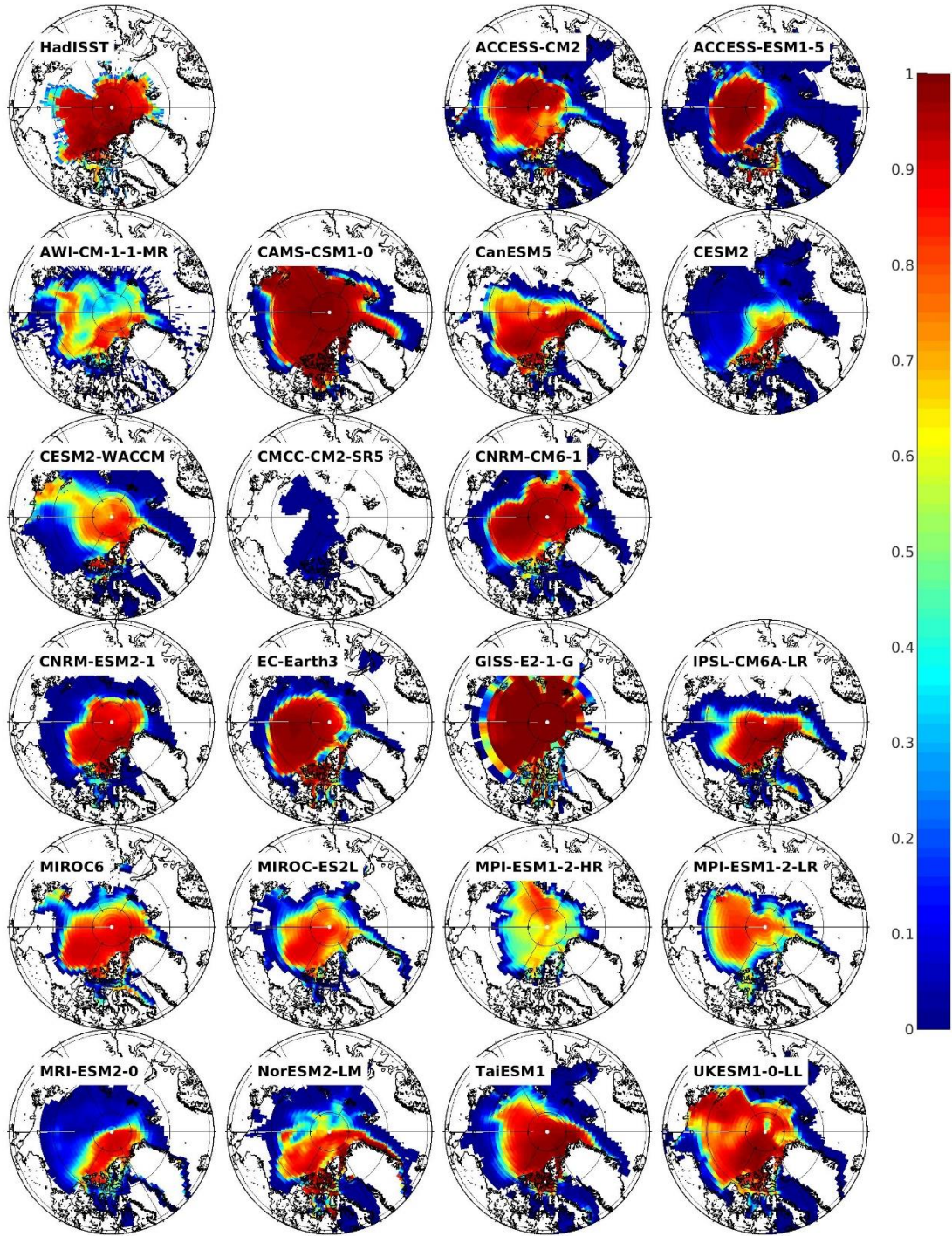


Figure 2.3.13. Sea ice concentration in the September of 2014 from HadISST and CMIP6 ESMs.

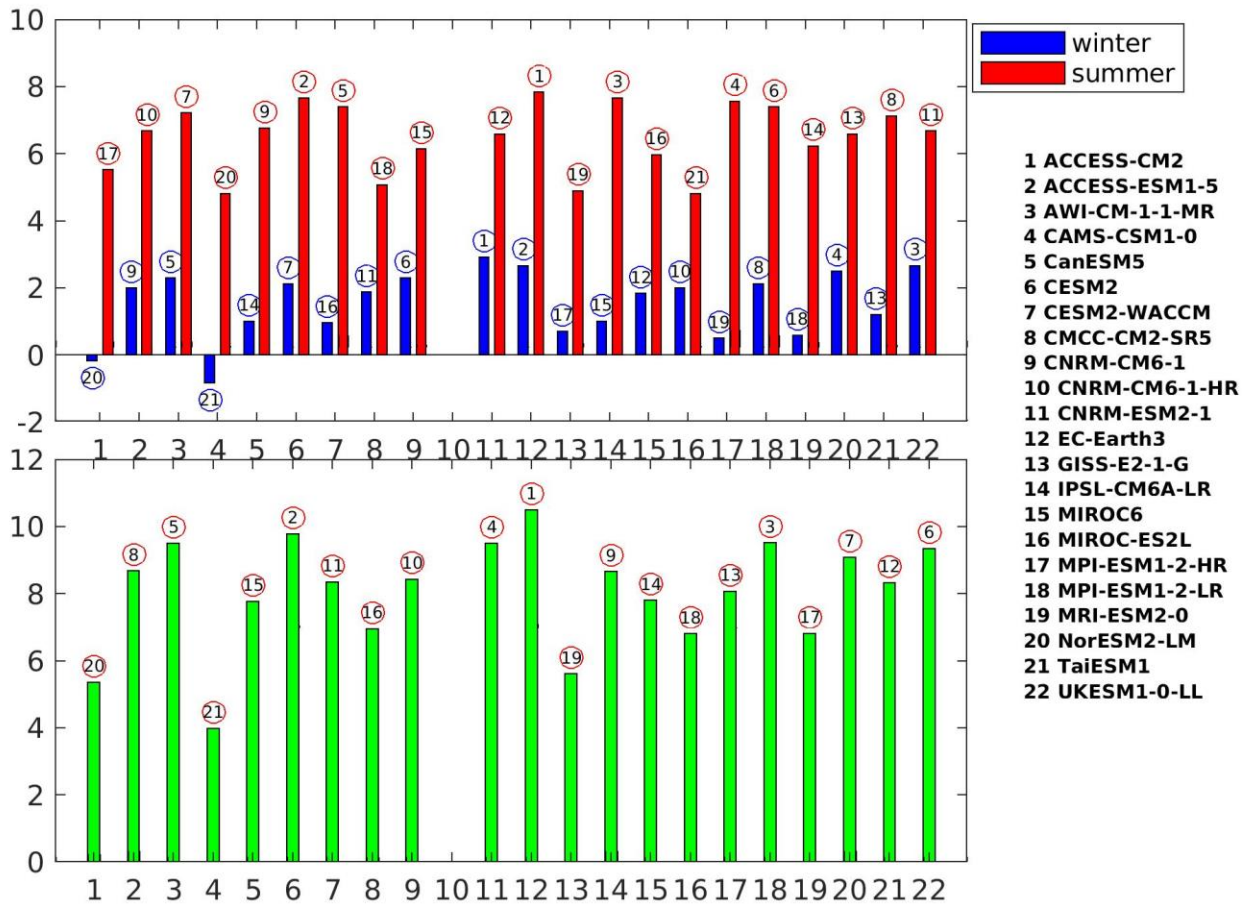


Figure 2.3.14. Performance score based on correlation coefficients (ice area: HadISST and CMIP6; top panel); combined performance score (bottom panel). Circled number is the ranking of the CMIP6 models indicated by the number on x-axis.

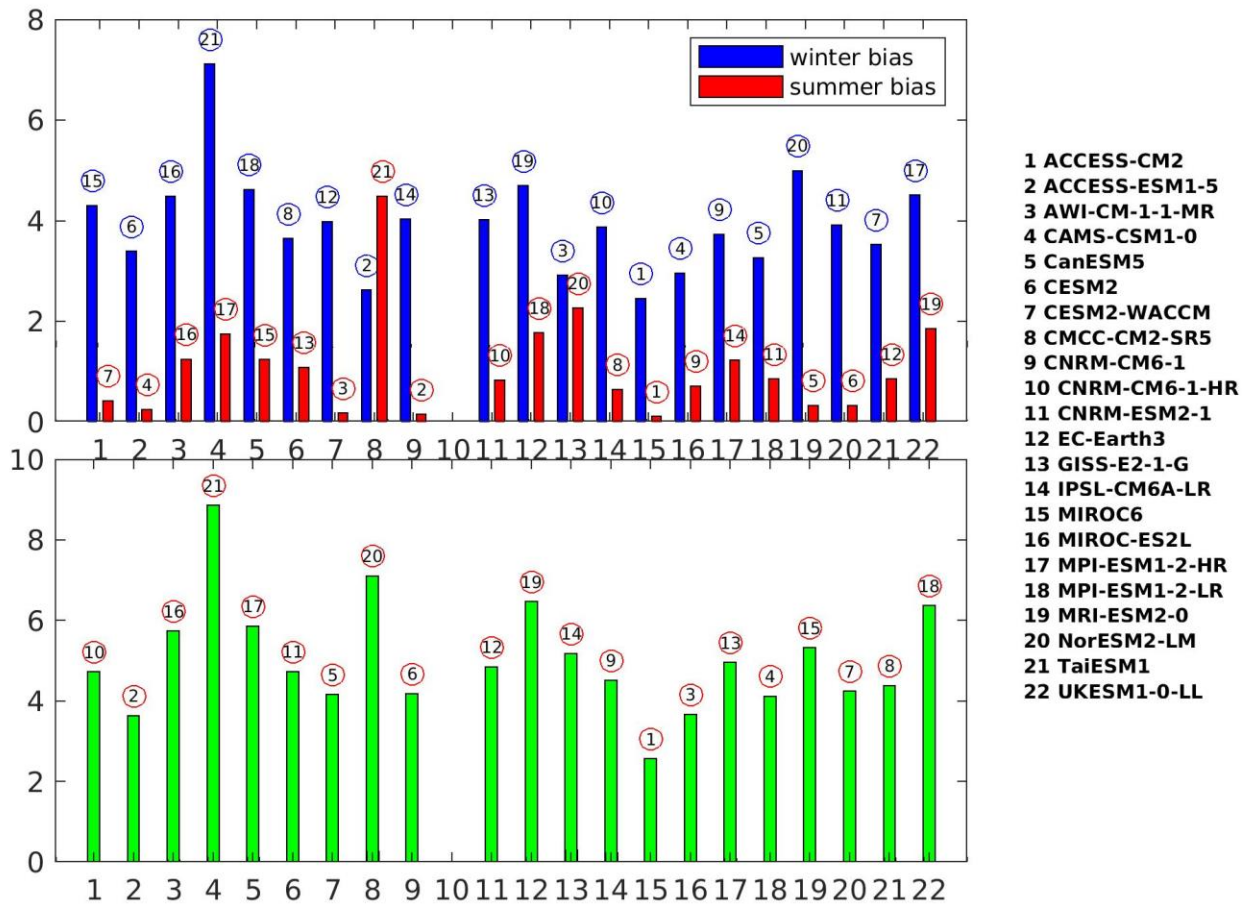


Figure 2.3.15. Model's error score based on ice area bias (top panel); combined error score (bottom panel). Circled number is the ranking of the CMIP6 model indicated by the number on x-axis.

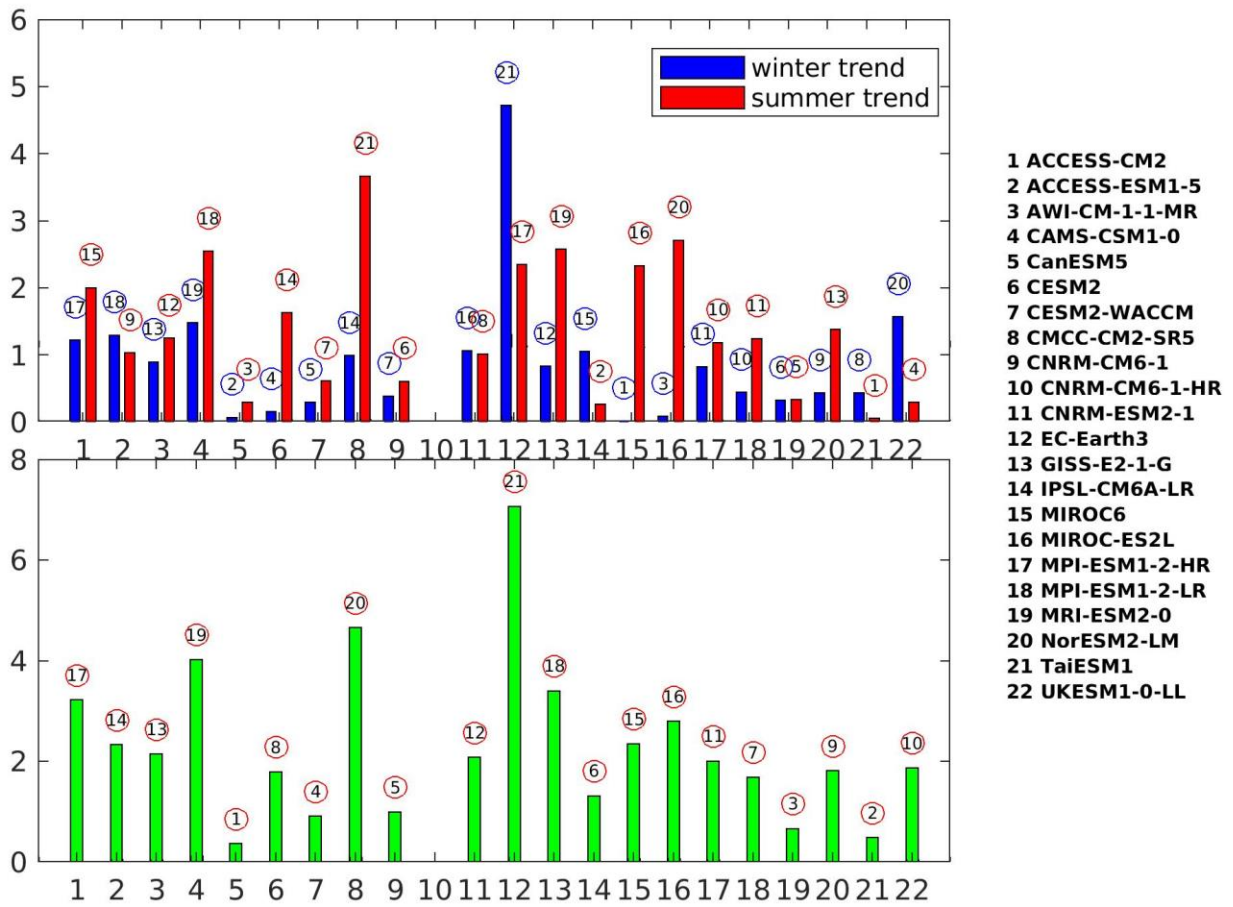


Figure 2.3.16. Model's error score based on ice area trends (top panel); combined error score (bottom panel). Circled number is the ranking of the CMIP6 model indicated by the number on the x -axis.

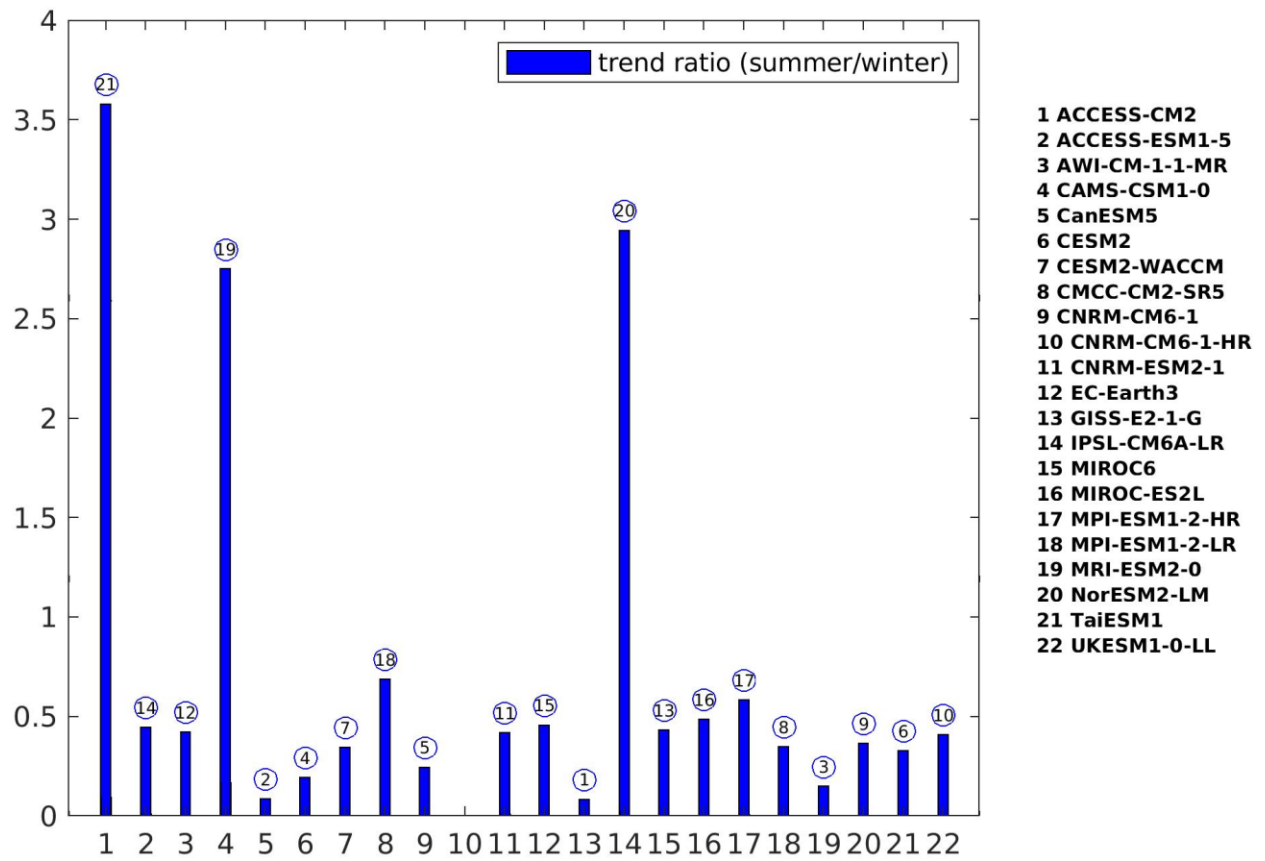


Figure 2.3.17. Model's error score based on ice area trend ratio (summer/winter). Circled number is the ranking of the CMIP6 model indicated by the number on the x-axis.

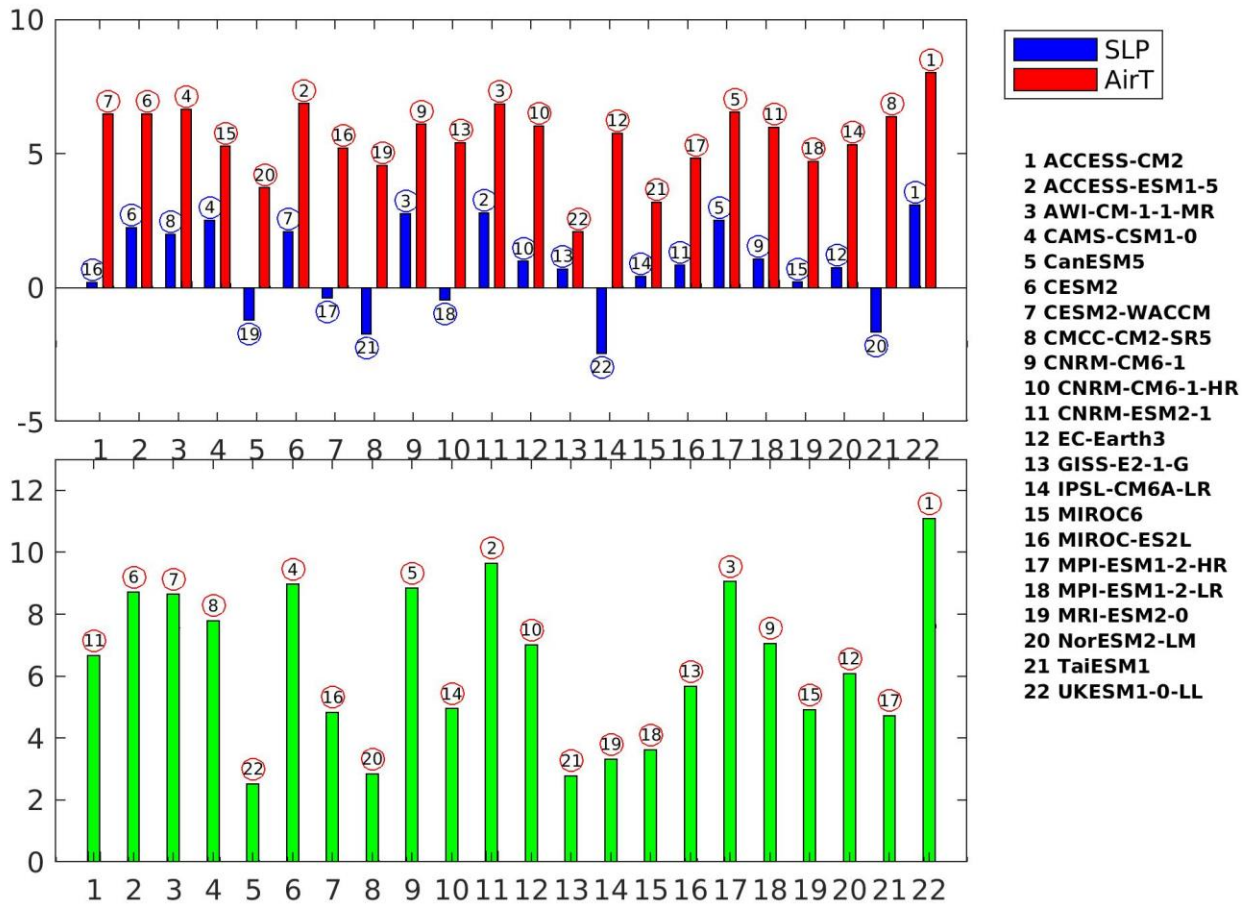


Figure 3.1 Model scores for SLP and AirT (top panel); combined model scores (SLP+AirT; bottom panel)

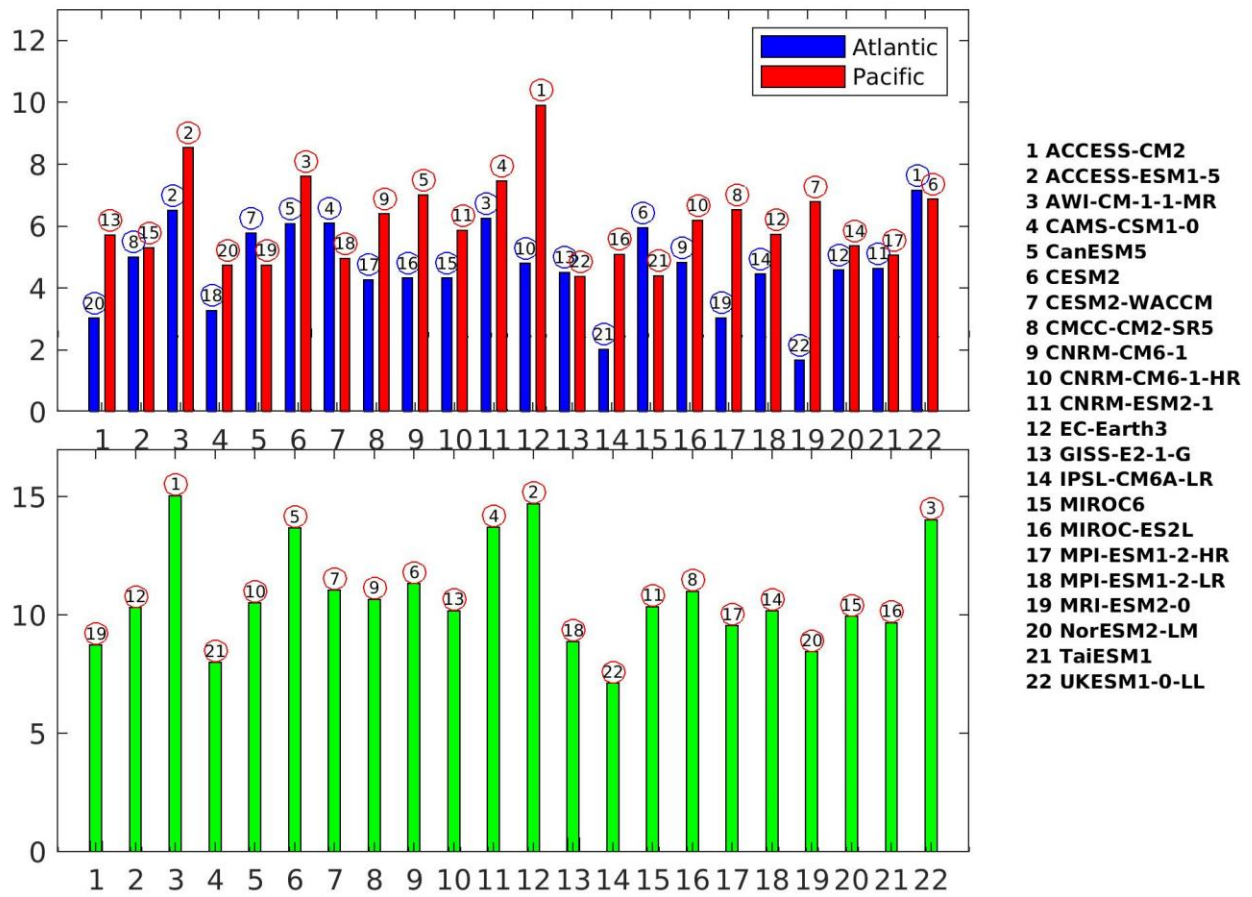


Figure 3.2 Model scores of SST for The North Atlantic Ocean (blue) and North Pacific Ocean (red, top panel); combined model scores SST in both regions (bottom panel)

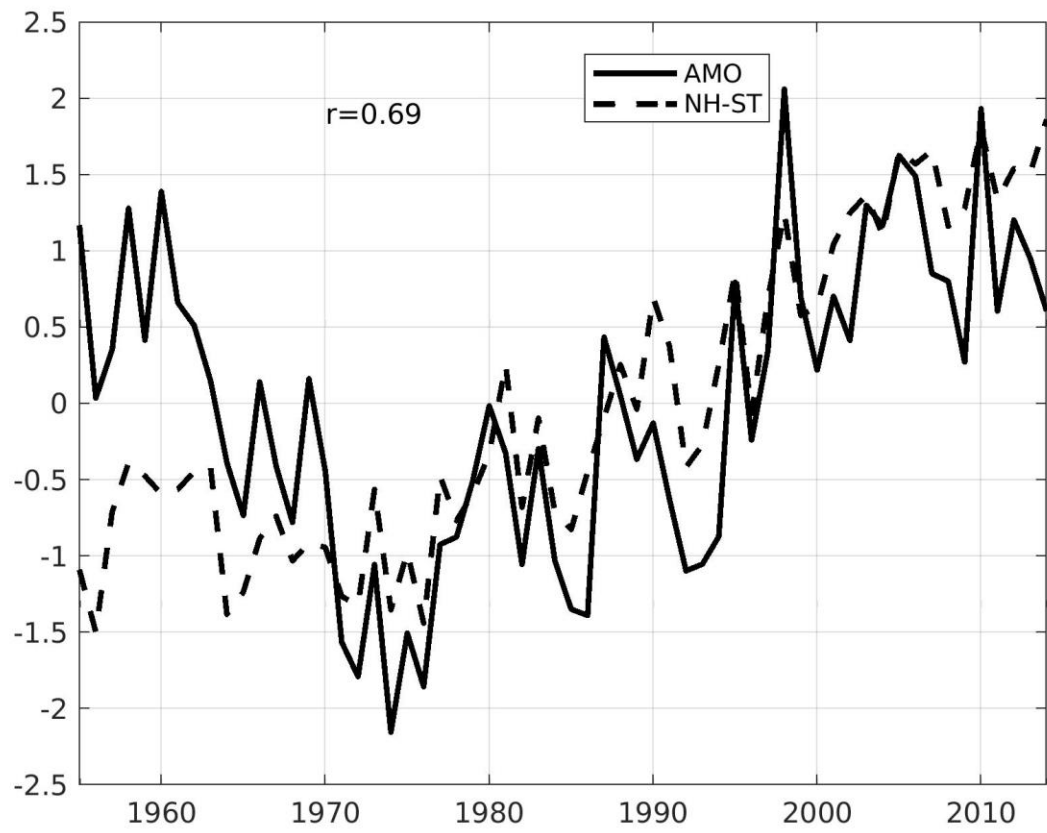


Figure 4.1 Timeseries of the AMO and NH-ST.